ANEXO I: TFM EXPANDIDO EN INGLÉS

CINÉTICAS DE CAPTURA DE CO_2 DEL AIRE BASADAS EN ADSORCIÓN

KINETICS OF ADSORPTION-BASED DIRECT AIR CAPTURE

Autor

Víctor Daniel Mercader Plou

Director

Jere Elfving (VTT Finland)

Ponente

José Ángel Peña Llorente

Máster en Ingeniería Química

ESCUELA DE INGENIERÍA Y ARQUITECTURA

2020

ABSTRACT

College of Higher Engineering and Architecture (EINA)

University of Zaragoza (UNIZAR)

Master's Programme in Chemical Engineering

Víctor Daniel Mercader Plou

Kinetics of adsorption-based Direct Air Capture

Master's thesis

2020

93 pages, 10 figures, 22 tables, 3 appendix

Keywords: Kinetics of adsorption, CO_2 adsorption, LDF, Zero-D model

Adsorbents are applied in direct air capture (DAC) technologies to extract CO_2 from the atmospheric air. Kinetics of adsorption are required to model and predict the behaviour of the adsorbent material in the adsorption process. The objective of the thesis is to study the different CO_2 adsorption kinetic models presented in literature, and to use the information to create a model to predict the CO_2 kinetic adsorption of a commercial amine-resin adsorbent. In addition, the objective is to validate the selected models with experimental adsorption results from thermal gravimetric analysis (TGA), fixed-bed adsorption and the amine-resin adsorption isotherm. Furthermore, the aim of the thesis is to compare the results of adsorption capacity and the adsorption kinetics obtained from TGA and the fixed-bed. Lastly, feasibility of two commercial zeolites, Zeolite 4Å as Zeolite 13X, as CO_2 adsorbents are tested.

Based on the literature survey, the selected models for CO_2 adsorption were based on the Linear Driving Force (LDF) adsorption approximation, including pseudo-first (LDF1), pseudo-second (LDF2) and Avrami and Veneman fitting models. In addition, the theoretical LDF models of Farooq & Ruthven and a model introduced by Perry et al. (1999) were applied.

According to the experimental results, the Veneman model was discovered to be the most accurate fitting model to predict the experimental results of CO_2 adsorption on the studied resin whereas from the theoretical models the model of Farooq & Ruthven predicted the kinetic adsorption behaviour on the resin the best. In addition, the diffusivity coefficient was found to differ between the TGA and fixed-bed adsorption processes at 400 ppm of CO_2 at 25ºC and 1.1 bar. Therefore, the global adsorption kinetic constant differs between TGA and fixed-bed adsorption processes. Considering the studied commercial zeolites, both Zeolite 4Å and Zeolite 13X showed CO_2 adsorption capacity, but for Zeolite 13X, regeneration difficulties at the desorption conditions were detected.

ACKNOWLEDGEMENTS

Firstly, I want to thank Jere Elfving and Jouni Hämäläinen for offering me the opportunity to be a part of their research team at VTT. I feel lucky to have been part of the research family of VTT and of having the opportunity of learning as much while improving my engineering skills.

Thanks to Jere and Jose Ángel for the help and academic support during the entire process of the thesis. Thanks to all the mates of VTT Jyväskylä, who were always kind to me and made me laugh even at the hardest moments.

One year has passed since I started my adventure in Finland and I feel like it has been only one day. I have fallen in love with this country and its people. Kiitos ja nähdään pian Suomi.

I want to say thank you to my relatives, my brother and father and especially to my mum. Thank you and good-bye grandfather.

Lastly thanks to my exchange and university friends and to my guild in Muniesa.

Contents

TABLES

Figures

LIST OF SYMBOLS AND ABBREVIATIONS

A_{column}	Cross sectional column area
A_{thermo}	Cross sectional thermopar area
C	Concentration
DAC	Direct Air Capture
D	Diffusivity coefficient
D_{colum}	Column diameter
D_{ef}	Effective diffusivity coefficient of the diffusivity compound in the pores.
D_K	Knudsen diffusivity coefficient
D_{Kef}	Knudsen effective coefficient
D_L	Axial dispersion coefficient, also referred as D_z
D_m	Molecular diffusivity coefficient
d_p	Pore diameter
D_p	Particle diameter
D_{pi}	Pore diffusivity coefficient
D_v	Viscous diffusivity coefficient
D_{vef}	Effective viscous diffusivity coefficient
FAO	Food and Agriculture Organization of the United Nations
J	Molecular flux
k_f	External mass transfer coefficient, also referred as k_g

K_n	Knudsen number, also referred as N_K
L_1	Length of thermopar
L_2	Length of column without thermopar
L_c	Column length
M_i	Molecular weight of compound i
MOF	Metal–organic framework
P	Total pressure
P_i	Partial pressure of compound i
q	Adsorption capacity
q_e	Adsorption equilibrium capacity
T	Temperature
R_c	Radio column
R_g	Ideal gases constant
r_p	Pore radius
R_p	Particle radius
S	Cross sectional area
v	Superficial velocity, also referred as u_o
vi	Interstitial velocity
V_c	Column volume
Vt	Thermopar volume

V_p	Volume of particle
v_p	Volume of pore
$\dot{V}$	Volumetric flow rate
Y_i	Molar fraction of the compound i

DIMENSIONLESS NUMBERS

Re_p	Reynolds of particle
S_c	Schmidt number
S_h	Sherwood
K_n	Knudsen number, also referred as N_K

GREEK SIMBOLS

ρ_f	Fluid density
ρ_b	Bulk density
ρ_s	Skeletal density
ρ_p	Particle density
μ	Fluid viscosity
λ	Free path
Ω_D	Integral collision coefficient
σ^2	Characteristic length (Å)
ε	Bed porosity, also referred as voidage
ε_p	Particle porosity

τ	Tortuosity

1 INTRODUCTION

The Food and Agriculture Organization of the United Nations (FAO) published a study in 2015 with the prognostic of necessity of food resources and population growth for 2050 (Bavec et al. 2017). The prognoses for 2050 indicate that the world population will increase to 9.1 billion which is almost two more billons than nowadays (Nations 2019). The increase of population will mostly be in the developing countries. In addition, the non-urbanized territory will be 20% lower than today (Wheeler et al. 2015). In order to supply the demand of food for the increasing population, the levels of food production will need to increase 70% (Wheeler et al. 2015). If this prognosis realizes, the traditional horticulture will not be able to supply the demand of food. In order to improve the yield and production of food, the horticulture technology needs to change (Bavec et al. 2017). According to Bavec et al. (2017) one of the new trends to improve the yield and productivity in horticulture is to apply the principles of sustainable intensification. The objective of these principles is to improve the yield and productivity of greenhouses and farms while respecting and conserving the environment.

1.1 Greenhouses intensification to supply the demand of food

The studies of S. A. Prior et al. (2003); Marchi, Zanoni, and Pasetti (2018); S. Prior et al. (2011) showed that the growing up process of vegetables is dependent of four principal factors: light exposition, water, soil composition and CO_2 concentration in the air. The studies assessed the effect of changing the common factors to find what is the contribution of the factors to the growing up process of vegetables. The absence of the required conditions decreased the growing up speed and productivity and were also able to cause the death of the vegetables. Finally, the studies found that increasing the concentration of CO_2 at levels higher than the atmospheric conditions (380-400ppm), the production edible vegetables increased more than 30%. The exact value of the increasing ratio depends of the studied vegetable specie and the CO_2, water and light conditions (S. Prior et al. 2011).

Different responses in the growth rate for two groups of vegetables with CO_2 supply were studied by S. A. Prior et al. (2003), S. Prior et al. (2011), Buijs and De Flart (2017) and

Kimball and Idso (1983). The increase in the growth rate for the first vegetable group under the given CO_2 supply was 33-40%, whereas for the second group the increase was 10-15%.

In their study, the conclusion was that the differences in the growth were caused because the photosynthetic pathways in the studied vegetable groups were not the same. The photosynthetic pathway is the compound responsible for the transport of CO_2 in the vegetable veins, being it an analogous to haemoglobin for human (Pessarakli 2005). Two photosynthetic pathways "C_3" and "C_4" are generally found in vegetables, with their nomenclature referring to the chemical composition of the compound. The growth rate registered for C_3 plants has a range of 33% to 40% in comparison to growth rate of 10% to 15% in photosynthetic pathway C_4. Therefore, the first group of studied vegetables in S. A. Prior et al. (2003), S. Prior et al. (2011), Buijs and De Flart (2017) and Kimball and Idso (1983) had a photosynthetic pathway of C_3, whereas the second group had the pathway of C_4.

Most of the horticulture species have the photosynthetic pathway of C_3. Therefore, CO_2 supply can apparently improve the production yield of horticulture (S. Prior et al. 2011). Some examples of vegetables with C_3 pathway are potato and rice, which both are basic ingredients in the human alimentation (Bavec et al. 2017). According to Kimball and Idso (1983) and Jin et al. (2009) each plant species has a CO_2 concentration range for optimal growth. However, CO_2 concentrations from 800 ppm to 1400 ppm have shown a 30% improvement in the growth rate of most edible vegetables in comparison to atmospheric CO_2 concentrations (Kimball and Idso 1983 & Jin et al. 2009). The impact of CO_2 concentration to the growth rate of vegetables with photosynthetic pathways C3 and C4 is presented in **Figure 1**. The figure shows the improvement in the rate of photosynthesis in relation to the CO_2 concentration referred to an atmospheric CO_2 concentration of 400 ppm (Kaiser and Drennen Thomas E. 1993).

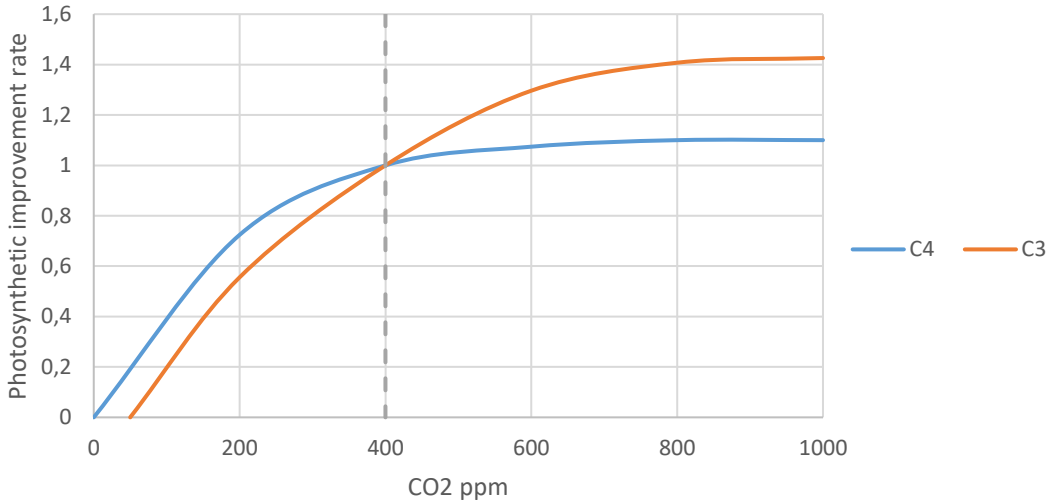

Figure 1. Rate of photosynthesis improvement for C3 and C4 photosynthetic routes for different CO_2 concentrations. The grey line is the atmospheric CO_2 concentration. Adapted from H. Kaiser et al. (1993).

Traditionally, use of greenhouses has been applied as a measure to increase the yield and production of horticulture (Bavec et al. 2017). Flexibility to choose the environmental conditions such as humidity, temperature, water source or CO_2 concentration inside of greenhouses is the key to increase the horticulture yield (Parajuli, Thoma, and Matlock 2019), although the conditions in the greenhouses consume more energy and water that the open-field farming (Bavec et al. 2017). The energy demand to maintain the proper environmental conditions in greenhouses has been supplied by oil, natural gas, dry ice for cooling and CO_2 supply, or electricity creating CO_2 emissions (Muñoz et al. 2008). Usually the production of vegetables in greenhouses has been increased by adding more water, chemical compounds, light and CO_2 derived from nonrenewable sources as fuels (Muñoz et al. 2008; Poudel and Dunn 2017). As a consequence, increasing the production rate of vegetables in greenhouses will increase the water demand and the use of fossil fuels resulting in increased CO_2 emissions (Bavec et al. 2017). Nowadays, the CO_2 concentration in the atmosphere is over 400 ppm which is over 100 ppm more than the CO_2 levels of the preindustrial period (280 ppm) (C.D. Keeling and T.P. Whorf 2001). A serial of different climatic horizons for emission reduction were promoted in the statement of the European

Commission (2014). The roadmap for the EU includes a reduction 32% in total greenhouse gas emissions by 2030, when compared to the levels in 1990 (European Commission 2014).

The main goal in horticulture is to increase the production of food, decrease the use of water while reducing emissions generated by maintaining the optimal conditions in the greenhouses (European Commission 2014; Bavec et al. 2017). One technology to supply the applicable temperature, water and CO_2 concentration without creating additional need for water and fossil fuels is Direct Air Capture (DAC) (Marchi, Zanoni, and Pasetti 2018).

1.2 DAC as technology and CO_2 supply in greenhouse intensification

Direct Air Capture was proposed as a technology to reduce excess atmospheric CO_2 by Lackner in 1999 (Sanz-Pérez et al. 2016). DAC is based in the uptake of CO_2 from airflow using physiochemical sorbents with CO_2 affinity. The non-adsorbed compounds are returned to the atmospheric air in the outlet flow and as a result, CO_2 concentration in the atmospheric air can be decreased (T. Wang et al. 2014). DAC is included into the negative carbon technologies, which have as an objective to obtain negative CO_2 emissions (Sanz-Pérez et al. 2016 & T. Wang et al. 2014). CO2 from DAC has potential for many applications; one of the most interesting points is that the final concentration of CO2 in the outlet flow can be chosen (Wang et al. 2014). The resulting CO2 flow can be used for high purity necessities such as pharmaceutic products, intermediate energy storage and to produce fuels. However, obtaining pure CO_2 from DAC has high operational costs and low economic profitability (Wang et al. 2014) .

Besides obtaining pure CO_2, DAC can also be applied in less exigent applications such as horticulture (Wang et al. 2014). Feasibility of DAC in supplying CO_2 for greenhouse applications was proven by T. Wang et al. (2014). The reduced purity demand of CO_2 decreases the operational costs and increases the profitability of the process (Wang et al. 2014). Implementing DAC as mechanism to provide CO_2 to greenhouses, the total balance of CO_2 emissions of the farming process can be reduced. In addition, DAC can be used to obtain water from the air, making easier to set up greenhouses in adverse environments such as deserts (Fasihi, Olga, and Breyer 2019). As a result, the arid soils could be exploited by greenhouse farming, which would decrease the requirements for arable land. Therefore,

applying DAC could be a possible part of solving the global food, water and emission problems (Wang et al. 2014).

A possible DAC technology is the use of aqueous sorbents. The use of aqueous hydroxide sorbents is common in the pulp and paper industry as an additional step to the Kraft process (Sanz-Pérez et al. 2016). A simplified scheme of Kraft CO_2 absorption process is presented in **Figure 2**. The technology is used to control the CO_2 emissions in pulp industry, and it includes an absorption step in which the sorbent is usually a water solution of NaOH. However, it can be replaced by more expensive absorbent KOH, but based on Sanz-Pérez et al. (2016), industrial use of KOH is not common.

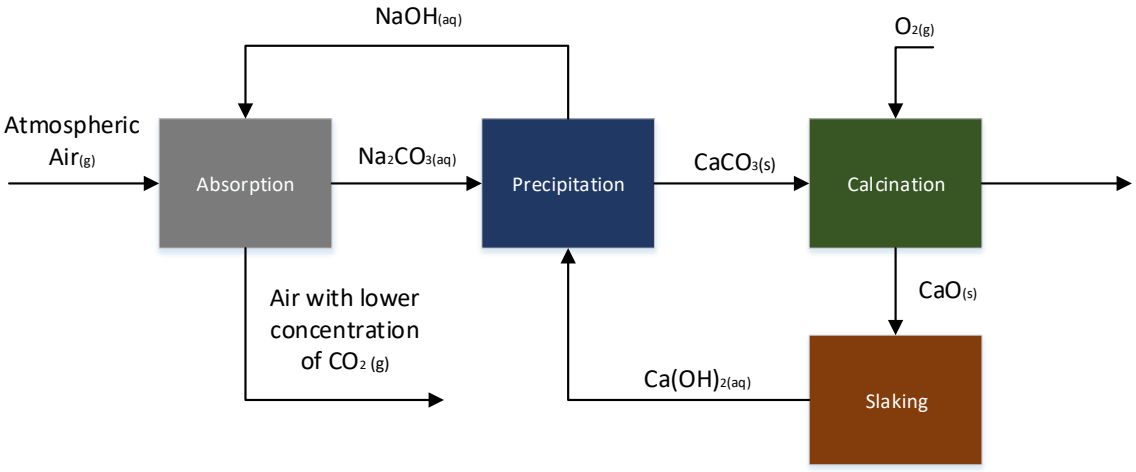

Figure 2. Scheme of a process for DAC aqueous sorbent based on the Kraft process in the pulp and paper industry. Adapted from Sanz-Pérez et al. (2016).

Main problems of the technology presented in the figure above are high energy demand and elevated operation costs during the calcination step. These drawbacks restrict the viability of utilizing the technology in DAC applications. However, the NaOH absorption step is assumable for the pulp and paper industry, because the CO_2 emissions generated during the main process are too elevated to be able to free them to the atmosphere. In addition, NaOH is a component that the main process already needs, and in the absorption process, the NaOH can be regenerated. Therefore, in DAC processes the actual tendency is to use solid adsorbents to remove the CO_2 from air (Sanz-Pérez et al. 2016). A comparison of the adsorption behaviour of different adsorbents presented in literature was done by Sanz-Pérez et al. (2016). In the studio was concluded that the general trend is that physical adsorption

contribution to the CO_2 uptake is lower were the adsorption capacity, sorption energy and adsorption enthalpy than chemisorption. The results showed physisorption is controlled by thermodynamic process and as result, low temperatures boosted the adsorption capacity of the physical adsorbents and also the capacity increases with the surface area. However, the chemisorption has a higher sorption energy creating stronger bonds. Chemisorption is usually boosted by temperature. As consequence of the chemical affinity between the adsorbate and adsorbent, the chemisorption processes are usually faster.

General trends in DAC adsorbent materials were studied in the work of Sanz-Pérez et al. (2016). Tendency is the use of silica functionalized with primary and secondary amines. Usually CO_2 capacity of physisorbents like silica is very low, so amine groups are included in the silica matrix in order to maximize the CO_2 capacity. The resultant composite is cheaper than to use a solid amine and the composite has more capacity than a common physical adsorbent. Yet, also other materials have shown good results after they have been functionalized with amines, as ionic resins, MOFs and new physisorbents are being developed, but they have not been studied as much as amine-silica compounds (Sanz-Pérez et al. 2016). An interesting field of study for these new materials is the kinetic characterization of the adsorption process. Kinetic study gives information about the behaviour of the adsorbent under the experimental conditions making it possible to predict the result of similar future experiments. In addition, kinetic data is essential for scaling up of sorption processes for industrial scale use (Perry et al. 1999).

1.3 Thesis objective

This thesis is focused to study different CO_2 adsorption kinetic models and to calculate the adsorption kinetic constant based on literature. The adsorbent materials studied are a commercial amine-resin, which is functionalized by primary and secondary amines and two zeolites with pore sizes of 13X and 4Å. The main objective of this thesis is to find the kinetic model able to predict the CO_2 adsorption process for the amine-resin sample. In addition, the viability of the zeolite samples as an adsorbent material in DAC is studied. The most important parameters for the adsorption kinetic models will be determined in order to predict the behaviour of the studied sorbents under different operating conditions. The experimental tests will be performed in a fixed bed and by Thermogravimetric Analysis (TGA), under

atmospheric CO_2 concentration and standard temperature that represents the conditions of a DAC scenario. Lastly, the results obtained from fixed bed and TGA are compared.

I. LITERATURE PART

2 KINETIC BASICS

A review of different models used in literature to model the adsorption kinetics of CO_2 on solid-amine compounds are presented in this chapter. The importance of the theoretical models is to obtain a theoretical approximation to predict the experimental results of the adsorption process. Thus, the theory helps to understand the adsorption behaviour found during the experiments. In addition, semi-empirical models will be introduced as a tool to solve the limitations in the theoretical-analytical solutions. A short introduction about the mechanisms of mass transfer for gas-solid adsorption systems will be introduced in order to clarify the order and contribution of each mechanism to the general adsorption mass transfer. In addition, the detailed information about the mass transfer will be introduced along the following subchapters.

Mechanism of diffusion in porous solids is a amply field studied by different authors such as Ruthven (1984) and Do (1998) and included in manuals of engineering such as Kunii and Levenspiel (1991) and Perry et al. (1999). Similar information and concepts can be found in all the books previously commented, and this chapter is based on these references.

The mass transfer in a gas-solid (G-S) adsorption column can be defined as a combination of the different individual mass transfer phenomena. Two main mass transfer groups can be differentiated based on the solid adsorbent particle, extraparticle and intraparticle. Intraparticle mass transfer includes the mechanisms of mass transfer occurring from the external surface of the particle to the interior of it. Intraparticle mechanism is affected by the selection of the adsorbent. Thus, for different solids the dominant internal kinetic mechanism can be different. The main intraparticle mechanisms are pore diffusion, surface diffusion and adsorption reaction.

In molecular diffusion into the pores, also referred as pore diffusion, the gas molecules are transported from the fluid film to the interior of the pores. The driving force is the difference

of concentration of the diffusive compounds in the diffusion media. This difference occurs between the part of gas film, which is in contact with the external solid face, and the concentration on the surface area of the pores. In surface diffusion, also referred as solid diffusion, the diffusive compound is attracted to the internal surface of the pore. After, the compound moves on the pore surface jumping to the next free site. The driving force is the difference in the concentration of the adsorbate between two points in the adsorbing phase. As for adsorption reaction, two main behaviours can be differentiated (Ruthven 1984). In physisorption the bonds adsorbate-adsorbent are based on the affinity of the adsorbate-adsorbent. Mostly, the bonds generated by physisorption are weak and nonspecific. In chemisorption, which is the other adsorption reaction, the bonds are based on chemical reactions, which makes the bonds stronger and highly specific in comparison to physisorption.

Extraparticle mass transfer includes the mechanism of mass transfer from the fluid phase to the external surface of the particle. Extraparticle mass transfer mechanisms are dependent of the design parameters of the adsorption equipment and of the fluid dynamic behaviour close to the particles. The main extraparticle mechanisms are external mass transfer and axial mixing.

In the external mass transfer an external fluid film resistance is generated when a fluid is in movement around the solid particles. The fluid film is dependent of the fluid dynamics. In the external mass transfer step, the diffusive compound must cross the fluid film to be able to contact the solid surface. The driving force is the concentration difference between the external boundary of the fluid layer and the fluid zone in contact with the external surface of the solid. Axial mixing can appear in non-ideal adsorption columns systems in which mixing occurs in the axial direction. The axial mixing is originated in fixed beds as result of the turbulences in the fluid when it crosses the void volume between particles in a fixed-bed. Axial dispersion diverts the flow behaviour to the ideal plug flow model and as result, the equations to define the ideal mass balance such as the continuity flow equation needs to be adjusted using a correction parameter. The adsorbate molecule generally needs to follow the diffusion steps presented in **Figure 3** to be able to be adsorbed (Perry et al. 1999). The figure describes the process of adsorption in a bed of adsorbent particles with an adsorbate gas phase crossing through the particle bed.

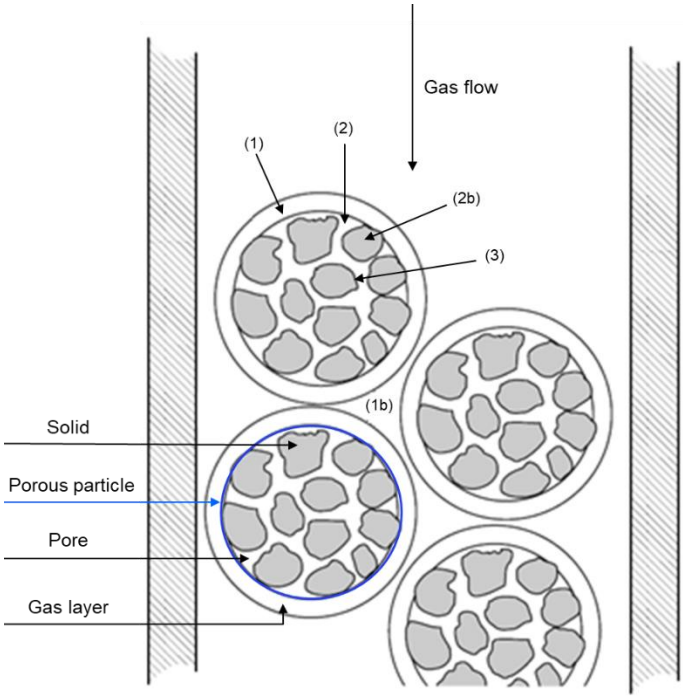

Figure 3. Mass transfer mechanisms in an adsorption column. (1) External mass transfer; (1b) Axial mixing; (2) Pore diffusion; (2b) Solid diffusion; (3) Adsorption reaction. (1b) is produced in parallel to (1). (2b) is produced in parallel to (2). Adapted from Perry et. al (1999).

As seen from Figure 3, the three mass transfer mechanisms are in serial, the order is external mass transfer, pore diffusion or/and solid diffusion and reaction on the internal surface of the solid. Thus, the slowest process will determine the global adsorption and will control the adsorption kinetics. In order to propose the kinetic model for CO_2 DAC system, the controlling step must be found. Therefore, the different mechanisms occurring during the adsorption processes will be described in more detail in the next subchapters.

2.1 Intraparticle diffusion

Along the intraparticle diffusion section, the different mechanism of transport that can occur into the particle will be discussed. The mechanism of intraparticle diffusion follow the Fick law (Eq. 1). Thus, the differences between the diffusivity coefficients described the variations in the intraparticle diffusion models.

$$J = -D\frac{\partial c}{\partial x} \quad \text{(Eq. 1)}$$

Where:

D	Diffusivity coefficient
∂c	Driving force, in this case referred to differential of concentration
∂x	Differential of the distance that the molecule must cross

2.1.1 Molecular diffusion or continuum diffusion

Molecular diffusion into the pores is observed when the pore size is much greater than the free path (λ) (Ruthven 1984). The free path is described as the free distance that a molecule of the diffusivity compound can go down before to collide with the walls of the pore (Do 1998). In the molecular diffusion model for a porous solid, the collisions of the diffusivity gas molecules with the walls of the pores are considered negligible (Pérez and Ariso 2008). The molecular diffusion in the pores is also called continuum diffusion because the model considers the diffusivity media as a continuum media (Do 1998). The continuum diffusion in porous solids considers that the pore diffusive media is the fluid phase inside the pores (Do 1998). The diffusion coefficient of gas 1 in gas 2 (D_{m12}) can be calculated using the approximation of Chapman-Enskog (Eq. 2) if the gas resultant is a binary non-polar mixture (Ruthven 1984). A binary non-polar mixture is a combination of two gases with low or non-polar charge such as the nitrogen and the carbon dioxide. Thus, Chapman-Enskog equation is applicable to the gas chosen to simulate the DAC, a mixture of 400 ppm of CO_2 in N_2.

$$D_{m12} = \frac{0.001858\, T^{3/2}(1/M_1 + 1/M_2)^{1/2}}{P\sigma_{12}^2\Omega_{D,12}} \quad \text{(Eq. 2)}$$

Where:

D_{m12}	molecular diffusion of gas 1 in gas 2 ($cm^2 \cdot s^{-1}$)

T	temperature (K)
M_1	Molecular weight of gas 1 ($g \cdot mol^{-1}$)
M_2	Molecular weight of gas 2 ($g \cdot mol^{-1}$)
P	Total pressure (atm)
σ^2_{12}	Characteristic length (Å)
$\Omega_{D,12}$	Integral collision coefficient (dimensionless)

D_{m12} only depends the operation conditions and the gas characteristics, the solid selection does not have any effect in D_{m12}.

In order to be able to use the Fick's law, tortuosity and particle porosity parameters have to be determined. Tortuosity corrects the effect of the random orientation of the pores in the solid. Thus, tortuosity parameter allows to calculate the diffusion coefficient taking in account the changes in the fluid dynamic into the pores originated by the random orientation of the pores. The tortuosity factor is characteristic of the solid chosen. The molecular diffusivity considering the tortuosity is presented at (Eq. 3) as D_p. (Ruthven 1984; Pérez and Ariso 2008)

$$D_p = \frac{D_m}{\tau} \qquad \text{(Eq. 3)}$$

Several theoretical approximations to calculate the tortuosity have been proposed in bibliography, but they usually show differences with values found by experimental determination (Do 1998; Perry et al. 1999). Thus, the advantage of the theoretical approximations for tortuosity is to obtain an illustrative value. Generally all theoretical tortuosity determinations consider that the tortuosity has a strong dependence of the porosity of particle value (Do 1998; Perry et al. 1999). The most common referred equations to determine the tortuosity are presented at **Table 1**, from Do (1998, p 397-398).

Table 1. Tortuosity factor approximations.

Monte-Carlo simulation	Weissberg Model	Bruggeman Model
$\tau = 1 + \frac{1}{2}(1 - \varepsilon_p)$	$\tau = 1 - \frac{1}{2}\ln \varepsilon_p$	$\tau = \frac{1}{\sqrt{\varepsilon_p}}$

Porosity of particle (ε_p) is a rate between the pore volume inside of the adsorbent particle and to the total volume of the particle (Ruthven 1984; Pérez and Ariso 2008). Additionally, ε_p can be determined using the skeletal density and the pore volume of the solid (Eq. 4). The estimation of pore volume (V_p) is calculated considering the pore as a cylindrical cavity with a pore radius approximately homogeneous (Eq. 5).

$$\varepsilon_p = \rho_s * V_p \; ; \; \rho_p = (1 - \varepsilon_p) * \rho_s \qquad \text{(Eq. 4)}$$

Where:

ρ_s	Skeletal density (kg/m^3)
ρ_p	Particle density (kg/m^3)
V_p	Pore volume per mass unit (m^3/kg)

$$\frac{V_p}{S_g} = \frac{\pi {r_p}^2 L_p}{2\pi r_p L_p} = \frac{r_p}{2} \qquad \text{(Eq. 5)}$$

Where:

Sg	Superficial area per mass unit
r_p	Pore radius
L_p	Pore length

As result of the corrections, the Fick law can be expressed as the (Eq. 6).

$$J = -\varepsilon_p D_p \frac{\partial c}{\partial x} \qquad \text{(Eq. 6)}$$

The previous equation can be rewritten by including the product of D_p and ε_p in a new parameter as an effective pore diffusion coefficient (D_{ef}) (Ruthven 1984; Pérez and Ariso 2008):

$$J = -D_{ef} \frac{\partial c}{\partial x} \; ; \; D_{ef} = \frac{D_m}{\tau} \varepsilon_p \qquad \text{(Eq. 7)}$$

2.1.2 Knudsen

Knudsen diffusion is observed when the pore diameter is smaller than the mean free path. Impact of the particles with the wall of the pore affects negatively in the diffusion, reducing the flux as consequence (Ruthven 1984; Pérez and Ariso 2008). Usually the Knudsen flow is found for mesoporous material under low total pressure and with pores in the order of 10 to 100 nm (Do 1998). In the study of Y. Yang and Liu (2019) the limit pressure boundary for Knudsen flow is >2.5 MPa. The diffusivity parameter for Knudsen diffusion D_K can be calculated as (Ruthven 1984):

$$D_K = 9700 \, r_p \left(\frac{T}{M}\right)^{1/2} (cm^2 s^{-1}) \qquad \text{(Eq. 8)}$$

Where:

r_p	Pore radius (cm)
M	Molecular weight of the diffusing component (g/mol)
T	Temperature (K)

As seen from (Eq. 8), D_K is only dependent of the temperature, the molecular weight of the diffusing species and of the pore radius. Additionally, the previous equation shows that the interaction between the different components diffusing is negligible and the flux of a component is independent from the rest of the species (Ruthven 1984; Pérez and Ariso 2008). The difference in the D_K as separation method has been studied in membrane studies (Nagy and Nagy 2019). Thus, for enough differences in D_K the porous media can be used to separate the components of a mixture (Eq. 9) (Nagy and Nagy 2019).

$$\text{Separation factor Knudsen} = \frac{J_i}{J_j} = \sqrt{\frac{M_j}{M_i}} \qquad \text{(Eq. 9)}$$

Where:

j	Compound that cross the solid
i	Compound retained

In order to take in account the tortuosity and porosity of the porous particle, the Knudsen effective diffusion coefficient presented at (Eq. 10) is deduced from (Eq. 8).

$$D_{Kef} = \frac{\varepsilon_p D_K}{\tau} \qquad \text{(Eq. 10)}$$

Writing the Fick law (Eq. 1) in terms of Knudsen diffusion (Eq. 10) the expression presented at (Eq. 11) is obtained:

$$J = -D_{Kef} \frac{\partial c}{\partial x} \qquad \text{(Eq. 11)}$$

Also, the Fick law for Knudsen diffusion (Eq. 11) can be expressed in terms of pressure as it is presented at (Eq. 12).

$$J = -D_{Kef}\frac{\partial c}{\partial x} = -\frac{D_{Kef}}{R_g T}\frac{\partial P}{\partial x} \quad \text{(Eq. 12)}$$

Where

P	Pressure of the diffusing compound
R_g	Gas constant
T	Temperature (K)

Knudsen number was created to be able to know if the diffusion is under Knudsen regime (Ruthven 1984). The Knudsen number is defined as:

$$K_n = \frac{\lambda}{d_p} \quad \text{(Eq. 13)}$$

Where:

d_p	Diameter of channel / pore (m)
λ	Free path (m)

As a result of the K_n three different regimes can be found (Do 1998):

K_n<<1: the viscous flow regime is applicable, and the behaviour can be predicted using the Poiseuille flow equation (Eq. 18). The model considers Newton law of viscosity and as result, the velocity of the fluid phase close to the pore is zero. Total pressure difference between the internal pore cavity and the gas on the surface are is high.

$K_n \approx 1$: For K_n with the same order that 1, the velocity close to the wall is not zero. Thus, both regimes have influence in the mass transfer.

K_n>>1: The concept of viscous flow is not applicable anymore, and the behaviour can be explained using the Fick law under Knudsen regime (Eq. 12).

From Perry et al. (1999) free path can be calculated as it is presented in (Eq. 14).

$$\lambda = \frac{3.2\,\mu}{P}\sqrt{\frac{R_g T}{2\pi M_1}} \qquad \text{(Eq. 14)}$$

Where:

λ	Free path (m)
μ	Viscosity of gas 1 (Pa·s)
M_1	Molecular weight of gas 1 (kg/mol))
R_g	Ideal gas constant, 8.314 (Pa·m^3/mol K)

Do (1998) calculated the minimum size of pore to be able to consider the Knudsen flow as the dominant mechanism (K_n>>1). As result of the study, it was concluded that the Knudsen flow is the dominant mechanism of diffusion for commercial mesoporous solids with a pore size lower than 50 nm. An alternative regime control classification can be founded in the engineering handbooks of Perry et al. (1999) and Pérez and Ariso (2008). The classification proposed is:

K_n<<1: Molecular diffusion regime

$K_n \approx 1$: For intermediate K_n the diffusion is controlled by both regimes.

K_n>>1: Knudsen regime

For $K_n \approx 1$ the coefficient of diffusion can be calculated using the equation proposed simultaneously by Evans, Watson and Manson and Scoth and Dullien (Eq. 15) Perry et al. (1999) .

$$\frac{1}{D_{ef}} = \frac{1}{D_{Kef}} + \frac{1}{D_m}\left[1 - \left(1 + \frac{J_2}{J_1}\right)\mathrm{Y}_1\right] \qquad \text{(Eq. 15)}$$

Where:

J_1	Molar flux of component 1
J_2	Molar flux of component 2

Y_1 Molar fraction of the component 1

In the specific application of DAC, the molar fraction of CO_2 is as low that the equation can be simplified as:

$$\frac{1}{D_{ef}} = \frac{1}{D_{Kef}} + \frac{1}{D_m} \quad \text{(Eq. 16)}$$

After comparing both classifications for Knudsen number, the conclusion is that the molecular diffusion and the viscous flow occur under same Knudsen regime as it is mentioned by Perry et al. (1999). In addition, contribution of viscous flow to the diffusion is always dominant over the molecular diffusion (Perry et al. 1999). Thus, the equations (Eq. 15) and (Eq. 16) are applicable under if the viscous flow is observed, the only step necessary is to replace D_m by D_v (viscous flow diffusivity coefficient).

2.1.3 Viscous flow

Viscous flow will appear when the difference of total pressure across the particle is elevated, as result the driving force is the difference of total pressure (Do 1998). This mechanism of diffusion is usually dominant in macroporous materials with a radius of particle between 10^{-7} and 10^{-5} m (for 1 atm and 20ºC) (Do 1998). The viscous diffusivity coefficient (D_v) can be calculated from Poiseuille´s equation presented in the manual of Ruthven (1984) as:

$$D_v = \frac{P{r_p}^2}{8\mu} \quad \text{(Eq. 17)}$$

Where:

P	Absolute pressure (dynes/cm^2)
μ	Viscosity (poise)
r_p	Pore radius (cm)
D_v	Viscous flow diffusivity coefficient (cm^2/s)

The Fick law (Eq. 1) in terms of viscous flux for a medium pore solid was proposed by Do (1998) and it is presented at (Eq. 18).

$$J_{vis} = -\frac{\varepsilon_p {r_p}^2}{8\mu\tau}\frac{P}{R_g T}\frac{dP}{dZ} = -\frac{\varepsilon_p {r_p}^2}{8\mu\tau} C R_g T = -D_{vef}\frac{dC}{dZ} \qquad \text{(Eq. 18)}$$

Where:

C	Total molar concentration (mol/m^3)
D_{vef}	Effective viscous flow diffusivity coefficient (m^2/s)

As a conclusion, viscous flow and molecular diffusion are two different mechanisms that coexist under the same Knudsen regime, appearing as dominant diffusion mechanism for Knudsen numbers << 1. The viscous flow will appear when the difference of total pressure across the particle is elevated and as a result the driving force is the gradient of pressure. The movement of the flow in the axial direction produces the differential of total pressure. Thus, the flux density depends of the differential of the pressure in the axial axis. On the other hand for molecular diffusion, the impulse force is the gradient of partial pressure or concentration of the diffusivity compound. Molecular diffusion is negligible in comparison with viscous flow if the difference of total pressure is elevated, meanwhile molecular diffusion will be dominant if the process is under constant pressure.

2.1.4 Surface diffusion (Solid diffusion)

The diffusive component is adsorbed firstly on the surface of the pore. After the adsorption, the adsorbate molecules start to vibrate. The vibration produces a “jumping effect” of the adsorbate molecules to the next adsorption empty site on the adsorbent surface. Surface diffusion appears in small size pores in which the predominant mechanism should be Knudsen. In addition, the superficial diffusion is highly dependent of the temperature, which promotes the vibration of the molecules. The way to identify if this mechanism is present is to compare the theoretical separation value for Knudsen diffusion with the real value estimated with the (Eq. 9). The concentration in the solid is calculated applying the

equilibrium of solid-gas solution using the Henry Law as is presented in the (Eq. 19). (Do 1998; Ruthven 1984; Perry et al. 1999)

$$C_s = K_H C_g \quad \text{(Eq. 19)}$$

Where:

C_s	Concentration of the diffusive component in solid phase
Cg	Concentration of the diffusive component in gas phase
K_H	Henry constant

The Henry constant is an thermodynamic equilibrium constant and it depends of the temperature and it can be obtained from the Van der Hoff equation as (Eq. 20) (Do 1998).

$$K_H = K_{H,\infty} exp(-\Delta H / R_g T) \quad \text{(Eq. 20)}$$

Where:

ΔH	Adsorption enthalpy (J/mol)

The diffusion coefficient for surface diffusion (D_s) is usually obtained from experimental data applying the Einstein theorem for the surface diffusion phenomenological coefficient (Valkovska and Danov 2000). The surface diffusion coefficient determination is complex and it has dependence of the isotherm behaviour (Valkovska and Danov 2000). As result and based in the literature about adsorption amine-resins, the surface diffusion was discard as the adsorption mass transfer mechanism. In addition, information about the determination of the diffusivity coefficient for surface diffusion can be found in Do (1998) and Valkovska and Danov (2000). The diffusion coefficients can be calculated for different temperatures from the Arrhenius equation and an example of the surface diffusion in particular is found in the (Eq. 21) (Do 1998).

$$D_s = D_{s\infty} exp(-E_s/R_g T) \quad \text{(Eq. 21)}$$

Where:

E_s	Activation energy (J)

The Fick law for surface diffusion will be descripted as:

$$J_s = -(1-\varepsilon_p) D_{s\infty} K_\infty exp\left(-\frac{E_s + \Delta H}{R_g T}\right)\frac{dC}{dz} \quad \text{(Eq. 22)}$$

2.2 External diffusion

The external diffusion is located in the fluid film around the particle. Fluid film resistance is generated when a fluid is in movement around the solid particles. Thus, the properties of the film are only dependent of the fluid properties. The thickness of that layer has a strong dependence of the velocity, temperature, pressure and viscosity of the fluid. The film creates an additional mass transfer resistance and as result it hinders the diffusion of the diffusivity compound from the fluid to the external surface of the particle. The mass transfer resistance can be the limitation step for some adsorption process such as DAC. The external diffusion is more relevant for processes with diluted adsorbate and it is almost negligible for processes with concentrated adsorbate. The mass transfer in that film can be defined with the linear driving force equation (Eq. 23) (Ruthven 1984).

$$\frac{\partial \bar{q}}{\partial t} = k \cdot a(c - c^*) = \frac{3k_f}{R_p}(c - c^*) \quad \text{(Eq. 23)}$$

Where:

k	Effective mass transfer coefficient of the diffusive compound
k_f	External diffusion constant of the diffusive compound
a	External surface are per unit of Vp (3/Rp for spherical particles)

q	Absorbed phase concentration average over a particle
c	Adsorbate concentration in the fluid phase
c*	Adsorbate concentration in equilibria in the solid

From the correlation of Ranz and Marshall in dimensionless terms, the effective mass transfer coefficient can be calculated as (Eq. 24).

$$Sh = \frac{2k_f R_p}{D_m} = \frac{0.357}{\varepsilon}\ {Re_p}^{0.64} {S_c}^{0.33} \qquad \text{(Eq. 24)}$$

Where

Sh	Sherwood number
ε	Void volume of adsorbent bed
Re_p	Reynolds of particle
Sc	Schmidt number

2.2.1 Axial dispersion

The axial dispersion coefficient includes the interparticle effect of the molecular diffusion and convection. In addition, the no uniformities in the flow velocity across the fixed-bed are included in the dispersion coefficient. The non-uniform velocity can generate gradients of velocity between the fluid in contact with the column walls and the fluid located in the bed center of the column. The gradient of velocity usually is bigger for big rates of diameter column-particle diameter, as result for big column diameters and small particles the velocity profiles can be elevated. However, axial dispersion origins the mix of the fluid flow in the axial axis and as result it affect also the concentration profiles in the column. The axial dispersion effect can be even more important for solids such as adsorbents as was suggest by Wakao, who determined an expression to calculate the dispersion coefficient including the effect of the porous adsorbent. (Ruthven 1984)

$$\frac{D_L}{2\upsilon R_p} = \frac{20}{\varepsilon}\left(\frac{D_m}{2\upsilon R_p}\right) + \frac{1}{2} = \frac{20}{Re_p Sc} + \frac{1}{2} \qquad \text{(Eq. 25)}$$

Where:

v	Interstitial velocity

2.3 LDF fitting models

The LDF fitting models are based into obtaining a mathematic correlation for the adsorption capacity along the experimental time. These models generate a constant that englobe the resistance to all mechanisms of mass transfer. Ideally, the constant obtained by fitting must coincide with the value constant of the dominant diffusion step or in case of all the mechanisms are relevant, the constant would include the contribution of all the mass transfer phenomena (Perry et al. 1999; Farooq and Ruthven 1990). As consequence, the value will be the same only if the impulse force has been referred to the same phase and the constant shows the same units (Perry et al. 1999). The use of fitting models is extended when the theoretical models are complex or the relations between the steps and species are not totally clear (Do 1998; Ruthven 1984; Perry et al. 1999). Additionally, the fitting model can be used when the dominant diffusion mechanism is not known. Thus, fitting models have as advantage that they can be used to explain the kinetic of adsorption of solid based in the adsorption results. The most referred fitting model in the engineering handbooks of Do (1998), Ruthven (1984) and Perry et al. (1999) is the Linear Driving Force (LDF). The LDF model consider the mass transfer as a linear expression that depends of a kinetic constant and a driving force between the amount of adsorbate in solid and the equilibria. The driving force can be expressed as concentration, capacity or partial pressure. In the (Eq. 26) is an example of the LDF from Ruthven (1984) and Perry et al. (1999), with the driving force is expressed as a differential of capacity.

$$\frac{\partial \bar{q}}{\partial t} = k_{LDF}(q - q^*) \qquad \text{(Eq. 26)}$$

Where:

q	Capacity of the adsorbent for a time t
q*	Capacity of the adsorbent in the equilibrium

A common trend for the calculation of the adsorption equilibrium capacity used in the LDF is determined from the adsorption isotherm based in the adsorption experiments carried out for the adsorbent (Buijs and De Flart 2017). The adsorption isotherm for an adsorption material is obtained from the combination of the adsorption curves for different partial pressures of the adsorbate at the same temperature (Ruthven 1984). Thus, the isotherm can predict the q_e of the adsorbent for different concentration of adsorbate in the inlet. The model of isotherm depends of the selection of the adsorbate, but the most common in kinetics of adsorption literature consulted are Langmuir, dual site Langmuir, Freundlich and Toth (Bos et al. 2018; Ben-Mansour et al. 2016; Shafeeyan, Wan Daud, and Shamiri 2014)

3 TRENDS IN ADSORPTION KINETICS

In this section, a summary of the most relevant information from literature for the objective of this thesis will be introduced. Additionally, the trends in adsorbent materials and the techniques used to carry out the adsorption test are studied. The main topic studied is the kinetics of adsorption in amine-resin compounds, specifically under DAC conditions. In addition, different models to simulate the adsorption kinetic of CO_2 are studied.

3.1 Adsorbent materials

Sanz-Pérez et al. (2016) included review of the DAC technology trends in adsorbent materials. The study indicated that the main trend in adsorbent materials is to use a porous material functionalized with groups that provide additional adsorption capacity in comparison with the non-functionalized matrix. In the case of material functionalized with amine materials, the amine generates chemical bonds that retain the CO_2 stronger than the physisorption bonds. Usually the base materials are physiosorbents with high porosity and surface area as silica or resin, or MOFs as a promising field (Armstrong et al. 2017; Ben-Mansour, Basha, and Qasem 2017; Darunte et al. 2016). The amine groups are fixed on the solid surface by bonds with different nature in depending of the matrix material (Darunte et al. 2016). The strongest bonds between the amine and the solid are generate if the amine polymerization process is carried out in contact with the solid matrix surface (Darunte et al. 2016).. In addition, the amount of amine that can be fixed by polymerization on the adsorbent surface is directly related with the surface area and porosity of the base solid (Darunte et al. 2016). The use of zeolites in CO_2 capture is not a new idea in physisorption, but the capacity obtained is lower that for materials functionalized with amines (Sanz-Pérez et al. 2016). However, the use of activated zeolites and the use zeolites with smaller pore size as molecular sieves has showed a new potential for this materials as CO_2 adsorbents (Sarker, Aroonwilas, and Veawab 2017). In addition, the use of metal organic frameworks with a solid matrix of zeolites have showed higher capacities than the conventional physisorbents, opening new possibilities in the DAC adsorption materials (Armstrong et al. 2017).

3.2 Techniques to characterize the kinetics of adsorption

The correct choose of the kinetic characterization techniques was one of the first questions during the planning of this thesis. As it will be introduced in the following paragraphs, the literature consulted mentioned mostly two techniques for the study of adsorption processes, Thermogravimetric analysis (TGA) and fixed-bed. However, other techniques has been reported such as BET. (Farooq and Ruthven 1990)

Thermogravimetric analysis (TGA) is a thermal analysis in which the mass changes of a sample are measure along the experiment time in function of the temperature (Basu and Basu 2018). Thus, the result of the experiment is usually the variation of mass of the sample along the time (Basu and Basu 2018). The applications of TGA in adsorption processes are commonly studied to determine adsorption capacity and kinetic parameters (Sanz-Pérez et al. 2016; Morin et al. 2017). TGA allows using flexible conditions for the experiments such as change the mass of sample, and high control of the temperature and pressure. In addition, the results of capacity can be determined directly from the measure of the mass sample variation along the experiment time (Elfving 2015; Morin et al. 2017).

Fixed-bed is a common method to obtain the data necessary in order to calculate the kinetics of adsorption of a system (Shafeeyan, Wan Daud, and Shamiri 2014; R. Veneman et al. 2016; Rens Veneman et al. 2015; Zarghampoor et al. 2017). Fixed-bed experiments can be carried out for higher flow rates than in TGA and the contact between the gas and the solid is more similar to industrial columns that the TGA (Shafeeyan, Wan Daud, and Shamiri 2014).

From the literature research was not found any conclusion about what techniques is more valid in order to obtain the kinetics of adsorption. Thus, the experiments for the samples were repeated using both devices, in order to compare the results. In addition, the decision was supported by the fact of the concentration of CO_2 in the kinetic of adsorption experiments found in the bibliography was very concentrated (>1%) in comparison with the 400 ppm of DAC scenario selected (Shafeeyan, Wan Daud, and Shamiri 2014). Therefore, some of the assumptions took by the authors could not be applicable anymore, such as Bos

et al. (2018), who used pure CO_2 considering the external resistance to the mass transfer negligible

3.3 Kinetic of adsorption models

Along the subchapter, the differences in the methods to calculate and to simulate the kinetic of adsorption on solid materials will be introduced, and in special the adsorption kinetics in amine resin materials. The biggest difficulty found during the research of literature was that kinetic adsorption models proposed by the authors did not follow a clear trend about how to use them and the differences in the device's conditions used to obtain the data. However, an additional hindrance was the non-transparency showed by the authors in the modelling report, such as showing just the results of the model or not specify what kind of kinetic constant was calculated. Those facts were also reported by Shafeeyan, Wan Daud, and Shamiri (2014). The second biggest goal was to identify the variables used in the adsorption kinetic determination such as the capacity or the properly diffusion coefficient and to unify the notation for the different authors. In addition the driving force was sometimes referred to the solid phase for example Perry et al. (1999) and others to the gas phase such as Farooq and Ruthven (1990). The results of the literature review were divided in two main Fickian model based and LDF fitting model based.

3.3.1 Fickian model applicability

Fickian Model was one of the most complex models found during the literature research. The Fickian Models are based into the equations presented in the subchapter 2.1 and they are used in the kinetic deductions in the manuals of (Do 1998; Ruthven 1984). The use of Fick models need a high knowledge of how is the adsorption along the solid, such as the modelling of the concentration profile in the particle in spherical coordinates (Shafeeyan, Wan Daud, and Shamiri 2014). Additionally a high detailed characterization of the adsorbent has to be carried out, such as the diffusion coefficients or the of (Ruthven 1984).In addition the mathematical model is complex because in it are included partial derivatives for the concentration of the adsorbate along the adsorbent radius (Ruthven 1984; Do 1998). One option to simplify the model is to consider a Zero-D model for the adsorption in the particle on which the driving force term as linear (Zamora et al. 2010). Thus, the concentration in

the solid is considered as an average of the concentration along the solid (Ruthven 1984; Perry et al. 1999; Do 1998). As result, the model obtained is the LDF model showed in the (Eq. 26). Some examples about the use of Fickian model as determination tool to calculate the kinetics of adsorption in CO_2 capture were reported by Serna-Guerrero and Sayari (2010) and T. Wang et al. (2016). In the study of Bos et al. (2018) was showed the dominance of the viscous diffusion and pore diffusion in the adsorption mass transfer. In addition the study confirmed the general trends proposed by Ruthven (1984) and Do (1998) for macro and mesoporous adsorbents. Thus, in this thesis the diffusivity coefficients for the Fickian model will be determined and the dominant intraparticle mass transfer will be proposed.

3.3.2 LDF models

LDF Models are several referenced in literature as a useful tool to simulate the CO_2 adsorption process, obtaining an accurate approximation to the experimental results (Choong and Scott 1998; Farooq and Ruthven 1990; X. Wang, Chen, and Guo 2015; Serna-Guerrero and Sayari 2010; Zarghampoor et al. 2017; Armstrong et al. 2017). The good results to simulate the experiments with a not high computational cost is probably one of the facts that makes the LDF one of the trends in kinetic adsorption modelling for CO_2 capture (Shafeeyan, Wan Daud, and Shamiri 2014). In this thesis, the LDF models have been divided in two main groups depending on how the adsorption kinetic constant is calculated. Thus, experimental models were referred to the models in which the adsorption kinetic constant is obtained from the experimental capacity and isotherm capacity results. In addition, theoretical methods were referred to the models in which the adsorption kinetic constant is determined mathematically from the extraparticle and intraparticle diffusion.

The simplest experimental LDF model is the Pseudo-First order model, presented at the (Eq. 27 (Bos et al. 2018). Besides of the simplicity of the model, the studies of Yang and Lee (1998) showed the accuracy in order to predict experimental results. In addition, in the studies of Serna-Guerrero and Sayari (2010) was concluded that the Pseudo-First order model is able to give a good prediction for materials with low surface coverage such as physisorbents.

$$\frac{dq}{dt} = k_{LDF1}(q_e - \overline{q}) \quad \text{(Eq. 27)}$$

Where:

q	Capacity (mol CO_2/kg adsorbent)
k_{LDF1}	Adsorption kinetic constant (s^{-1})
t	Time (s)
q_e	Equilibrium capacity
$\bar{q}$	Capacity average

Bos et al.(2018) considered Pseudo-Second order model showed a better mechanistic proposal for the dry reaction of two molecules of amine with one of CO_2. The model in presented at the (Eq. 28, as it can be observed that the capacity differential is eleveted to square. In the study of Guerrero and Sayari (2010) was concluded that for their CO_2 adsortpion process with an amine funtionalized silica the Pseudo-Second order was able to predict better adsroption when the surface coverage increased. In addition, the concentration of CO_2 used in the adsorption study of Guerrero and Sayari (2010) was 5%. Additionally, for the lower concentration of CO_2 studied in this thesis in comparison with the study of Guerrero and Sayari (2010) could imply that the phenomena of surface coverage will not appear.

$$\frac{dq}{dt} = k_{LDF2}(q_e - \overline{q})^2 \quad \text{(Eq. 28)}$$

Where:

- k_{LDF2}: adsorption kinetic constant ($kg \cdot mol^{-1} \cdot s^{-1}$)

As an alternative when both of the previous models are not accurate enough to the experimental results is the Avrami model (Serna-Guerrero and Sayari 2010). The Avrami model has been typically used for crystallization (Sha et al. 2011), but recently studies have showed the its potential in CO_2 capture modeling (Jung, Park, and Lee 2018; Serna-Guerrero

and Sayari 2010). In the Avrami model presented at (Eq. 29), the parameter n can be a fraction or an integer number and the variable time is included. Thus, the inclusion of the time in the Eq. 29 is able to fit better the model to the time axis and n parameter allows fitting better the equation to the slope of the curve.

$$\frac{dq}{dt} = k_A{}^n t^{n-1}(q_e - \overline{q}) \qquad \text{(Eq. 29)}$$

Where:

n	Adjust parameter of Avrami equation (dimensionless)
k_A	Avrami's adsorption kinetic constant (s^{-1})
t	Time (s)

The previous models presented at (Eq. 27) and (Eq. 28) were modified in the studies of Rens Veneman et al. (2015 & 2016) about CO_2 adsorption on a supported amine. The modification included the partial pressure of the adsorbate giving as result the ((Eq. 30). Rens Veneman et al. (2015 & 2016) found that the modified model was able to predict better the adsorption of CO_2 on an amine adsorbent in comparison with the prognosis of the (Eq. 27) and (Eq. 28).

$$\frac{dq}{dt} = k_{V1} p_{CO_2}(q_e - \overline{q}) \quad ; \quad \frac{dq}{dt} = k_{V2}\, p_{CO_2}(q_e - \overline{q})^2 \qquad \text{(Eq. 30)}$$

Where:

k_{V1}	Adsorption kinetic constant for LDF1 ($Pa^{-1}\cdot s^{-1}$)
k_{V2}	Adsorption kinetic constant for LDF2 ($Pa^{-1}\cdot s^{-2}$)

Various authors have proposed a theoretical determination of the adsorption kinetic constant based in LDF model (Eq.27) such as Farooq and Ruthven (1990) and LDF includes in Perry et al. (1999). In the LDF model proposed by Farooq and Ruthven the capacity is referred to the fluid phase and it is expressed in units of mol $_{CO_2}$/m^3. In addition, the first term of the equation includes the external mass transfer resistance, the second includes the macropore

diffusion resistance and the last one is referred to the micropore diffusivity. The model of Farooq and Ruthven (1990) is valid for linear isotherms and also a reasonably good approximation for non-linear systems Shafeeyan et al. (2014). The Farooq and Ruthven LDF constant determination is presented at (Eq. 31).

$$\frac{1}{k_i} = \frac{R_p q_0}{3 k_f c_0} + \frac{R_p^2 q_0}{15 \varepsilon_p D_{pi} c_0} + \frac{r_p^2}{15 D_{\mu i}} \qquad \text{(Eq. 31)}$$

Where:

k_i	Kinetic constant for LDF1 (s^{-1})
R_p	Particle radius (m)
q_0	Equilibrium capacity (mol_{CO_2}/ m^3)
c_0	Equilibrium concentration (mol_{CO_2}/ m^3)
k_f	External diffusion constant of the diffusive compound (m/s)
D_{pi}	Macropore diffusivity effective coefficient (m^2/s)
$D_{\mu i}$	Micropore diffusivity effective coefficient (m^2/s)
ε_p	Porosity of particle
r_p	Pores radius (m)

The LDF constant included in Perry et al. (1999) is presented at (Eq.32). has the same units for the adsorption capacity that (Eq. 27). The LDF Perry et al. (1999) is referred in this thesis as Perry's model.

$$k = \frac{15 \Psi (1 - \varepsilon) \varepsilon_p D_{pi}}{\Lambda R_p^2} \qquad \text{(Eq. 32)}$$

Where:

k	Kinetic constant for LDF1 (s^{-1})
D_{pi}	Pore diffusivity effective coefficient (m^2/s)
Ψ	Correction factor (dimensionless)

R_p	Particle radius (m)
Λ	Partition ratio (dimensionless)
ε_p	Porosity of particle
ε	Bed porosity

II. EXPERIMENTAL PART AND MODELLING

During the thesis different test were carried out, the object of them was to find the relevant properties needed in the adsorption kinetic modelling and to compare the results obtained from TGA and fixed-bed devices. In addition, the result from the adsorption kinetic models calculated from the diffusivity coefficients will be compare with the kinetic fitting models. Additionally, the adsorption kinetic constants obtained from the models will be listed and discussed. The equipment, techniques and materials used will be presented along this chapter. The adsorbent studies were a zeolite of 4Å, a zeolite of 13Å and the same amine-functionalized resin that was used in this work as in Elfving et al. 2017. In this thesis the samples will be referred to as Zeolite 4Å, Zeolite 13X and amine-resin.

4 DESCRIPTION OF DEVICES AND TECHNIQUES

4.1 Voidage determination

The void volume of the fixed-bed is an important parameter that is needed during the modelling of the system (Shafeeyan, Wan Daud, and Shamiri 2014). The void volume in the packed bed plays an important role in the external mass transfer and in the temperature distribution. The free volume between the particles can determine the fluid dynamic behaviour of the gas flow affecting the external diffusion coefficient, as it was showed at in the Sherwood Number and the axial dispersion parameter. The measurements from the F fixed-bed were taken using LabVIEW and processed by MATLAB R2018b and Excel.

The information necessary about how to carried out the experiments and the literature basics were obtained from the studies of Kunii and Levenspiel (1991). In addition the voidage is usually calculated using the Ergun equation (Eq. 33) (Zarghampoor et al. 2017). The voidage is characteristic of the solid as mass of shape and it has dependence of the temperature. The

determination of this parameter was carried out in the fixed bed descripted in **Figure 5**, with 0.05428 mg of amine-resin and the gas used was pure N_2. The steps followed were:

Firstly, pressure drop of the empty column was measured in order to know the contribution of the components of the column to the total pressure drop. The conditions of the experiments were representative of the adsorption-desorption process are included in the **Table 2** :

Table 2. Experimental conditions for the empty column.

$\dot{V}$ (L(STP)/min)	u_o(m/s)	T(ºC)
0.1	0.0262	25, 100
0.25	0.0655	25, 100
0.5	0.1310	25, 100
1	0.2620	25, 100
1.5	0.3930	25, 100
2	0.5240	25, 100

Where:

$\dot{V}$ (L/min): Volumetric flow rate of $N_{2(g)}$

T(ºC): Temperature of the fixed bed.

u_o(m/s): surface velocity

In second place, pressure drop was measure for the fixed bed charged with the amine-resin particles following the method proposed by Kunii and Levenspiel (1991). The methodology is divided into two stages. First, pressure drop was measured increasing the flow rate from zero to the higher value of the **Table 2**, theoretical result can be observed as line (1) in **Figure 4**. Second, the pressure drop was measured from the upper value of flow rate to zero, line (2) in **Figure 4**. An ideal result of the method is presented at **Figure 4**.

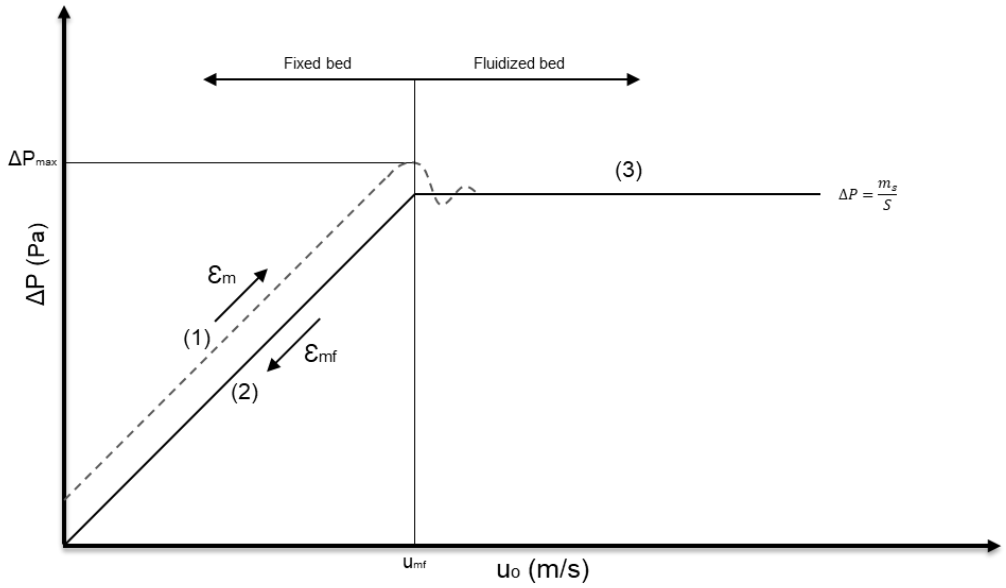

Figure 4. Pressure drop for a bed of solid particles. Adapted from Kunii and Levenspiel, Fluidization Engineering (1991).

From the **Figure 4** the superficial velocity of minimal fluidization can be obtained, it is the point in which the behaviour of the bed change from fixed bed to fluidized bed. Graphically the change is showed as the intersection of fixed bed behaviour (line 2) with fluidized bed behaviour (line 3). In addition, the point of minimal fluidization fulfils the conditions of fixed bed and fluidized bed. Thus, the rest of parameters were calculated solving in the minimal fluidization point the next equation system.

Ergun equation under minimal fluidization conditions (fixed bed behaviour):

$$\frac{\Delta P_{mf}}{L_{mf}} = 150\frac{(1-\varepsilon_{mf})^2}{{\varepsilon_{mf}}^3}\frac{\mu}{(\Phi D_e)^2}u_m + 1.75\frac{(1-\varepsilon_{mf})}{{\varepsilon_{mf}}^3}\frac{\rho_f}{(\Phi D_e)}{u_m}^2 \qquad \text{(Eq. 33)}$$

The previous equation can be simplified for $R_{ep} < 20$ as:

$$\frac{\Delta P_{mf}}{L_{mf}} = 150\frac{(1-\varepsilon_{mf})^2}{{\varepsilon_{mf}}^3}\frac{\mu}{(\Phi D_e)^2}u_m \qquad \text{(Eq. 34)}$$

Where:

ΔP_{mf} Pressure Drop

L_{mf}	Length of the bed
ε_{mf}	Porosity of the bed
μ	Viscosity of fluid
u_m	Surface velocity
Φ	Sphericity
D_e	Equivalent diameter

As the particles of amine-resin are spherical $\Phi = 1$

Pressure drop for fluidization regime was obtained by applying the equilibrium of forces Newton law at minimal fluidization conditions:

$$\Delta P_{mf} = \frac{m_s}{S} \qquad \text{(Eq. 35)}$$

4.2 Physical properties of the adsorbent material

The humidity of the samples supplied was measured by a standardized test used in LUT analytic laboratories. Firstly, a watch glass chosen as crucible for the test was introduced in the oven over 100ºC for 1 h and later it was tempered in a desiccator and weighted. The samples were weighted on the crucible on a high precision balance. Then, the samples on the glass were introduced in the oven at 100ºC along the night. After the drying process, the samples needed be cold down in a desiccator for 15-20 min. As last step, the weight was measured on the precision balance and the differences in the weight were registered. The differences in the weight were considered as moisture.

AutoPore IV 9500 V1.09 Hg pycnometer was used to determine the porosity, tortuosity factor and skeletal density of the amine-resin, Zeolite 4Å (pellet) and Zeolite 4Å (powder). The Hg pycnometer used pressurized mercury to fill the pores of the adsorbent sample. The amount of mercury introduced was related with the pore volume and size by the equipment. From the data obtained the equipment was able to calculate characteristics of the adsorbent such as porosity, tortuosity, bulk density, skeletal density, pore volume. Two samples of each adsorbent were tested, one was analysed directly with the moisture and the second a pre-treatment was done before to carry out the experiment. The pre-treatment had as objective to regenerate the sample, desorbing all the moisture and gases adsorbed on the solid. In addition, pre-treatment samples were dried in a vacuum oven at 100ºC for 2 hour and later the samples were cold down in a vacuum desiccator. Additionally, the cold down process had as first step removing the gases with Argon and later it was vacuumed.

Bulk density was measured experimentally using the physical relation between the mass of solid that occupied a known volume. The bulk density measurements were carried out at VTT Jyväskylä installations and the AutoPore corroborated the results.

In order to be able to observe the temperature dependence of the adsorption mechanism and the kinetic constants the experiments were carried out for different temperatures. Additionally, bed voidage experiments were carried out for the fixed bed device, the objective was to determine the characteristic parameters from the fixed bed and obtaining

more information about the solid. Particle density was calculated from the skeletal density with (Eq. 4).

4.3 Capacity characterization

The capacity of the adsorbents is one of the most important parameters in order to choose the adequate material for the DAC equipment. The capacity of the adsorbent along the time of experiment, and the equilibrium capacity are needed to calculate the adsorption kinetic constants. The measure of the adsorption capacity was characterize using the TGA and Fixed bed. Data analysis of the capacity was carried by similar method as in (Elfving et al. 2017) adapted to the tests experimental conditions of this thesis. The capacity data analysis is presented at the Appendix I.

TGA experiments were carried out in a thermal analyser model Netzsch STA 449 C Jupiter. The gases purity used during the experiments were N_2 grade 5.0, a mix of CO_2/N_2 of 1% with grade 4.0 and He grade 4.6 as a protective gas. The pure N_2 was used to dilute the mix of CO_2/N_2 until the CO_2 concentration of 400 ppm. Environics series 2000 computerized multi-component gas mixer made the dilution of 1% CO_2/N_2 to 400 ppm at 1.1 bar. The crucible sample cups dimensions were 1 cm height and 4 mm of diameter and the crucible material was solid Al_2O_3. A blank reference sample was carried out for the TGA adsorption recipe with the empty cup. The blank reference was used by the TGA to remove the contribution of the crucible in the adsorption process. The gas conditions in the outlet of the mixer were a gar flow rate of 50 ml/min. The value of flow rate was selected in order to satisfy the limitations of both devices, for TGA the max flow inlet was 50 ml/min and the minimum flow rate in the outlet of the mixer was 50 ml/min. Thus, both devices were working in the limit of their safety range. The mass of the samples was chosen based in the limitations of the internal balance of the TGA and the recommendations of the TGA technician. Thus, the mass between solids were not exactly the same, because the big differences in the density of the solids and the size of particle.

The TGA amine-resin samples were divided in two group, the first one was analysed directly without any pre-treatment and for the second group before to the adsorption test a regeneration step was carried out. The idea was to compare the effect of the gases adsorbed on the non-pre-regeneration samples with the samples pre-regenerated. Pre-regeneration step was carried out in a laboratory oven at 100ºC for 2h, after they were cold down in a laboratory desiccator for 15 min at room temperature. In addition, two different mass of resin

sample were tested, approx. 6 mg and 10 mg, for both groups of the amine-resin samples. The two mass allowed determining the effect of mass sample in the TGA adsorption process. The adsorption step was carried out at 25ºC, 1.1 bar for 12 h and a flow rate in the inlet of 50 ml/min with CO_2 concentration of 400 ppm. Desorption step was carried out at 100ºC, 1.1 bar for 5 h and same flow rate in the inlet than in the adsorption step. The heating process speed was 10 K/min.

The pre-treatment of regeneration was not carried out in the TGA because of the technical limitations found between the mixer and TGA. The fact of the mixer was working in the lowest limit conditions of outlet flow and with low concentrations of CO_2 complicated the properly control of the flow rate in the outlet. It was found that the internal controller of the mixer needed approximately three turning on and off trials before to be able to have an initial point of concentration that made the controller allows to converge to the properly concentration of 400 ppm in the outlet. On the other hand, the TGA inlet needed to be open during transition from the regeneration with N_2 pure to the adsorption conditions. Following the advice of the responsible of the device, the idea of to use first the N_2 as regeneration and later CO_2 was discard. The explanation was that the TGA balance was too sensible to support the changes in the inlet flow and concentration from the trials of the mixer to be able to converge to the properly concentration. In special during the transition from the pure nitrogen to the adsorption mixture. As result of the limitations of the equipment available, an external pre-treatment of the samples al 2h laboratory oven was proposed for the amine-resin samples. However, the zeolites did not have a pre-treatment because the hydrophilic behaviour of the zeolites was more elevated that the solid of the desiccator. Thus, the zeolites were able to adsorb water from the desiccator as it is showed in the humidity test results. The TSA adsorption and desorption conditions for the zeolites followed the same recipe that for the amine-resin samples, the mass of Zeolite 4Å was 5.66 mg and 30.95 mg for the Zeolite 13X. The TSA desorption conditions were 100ºC, 400ppm of CO2 and 1.1 bar of pressure. The temperature of 100ºC was founded in this thesis as the best to obtain a complete desorption, additionally this behaviour was reported in (Elfving et al. 2017).

Fixed-bed adsorptions were carried out at VTT installations in a lab scale fixed-bed device designed by VTT. The dimensions of the column were 4.7 cm of length and 9 mm of diameter and the material was solid stainless steel. The column is heated by either adsorption

(cool) or desorption circulation (hot) in the jacket. The heat is transferred to the sample through the jacket wall. The column dimensions and measurement points are presented at **Figure 5**.

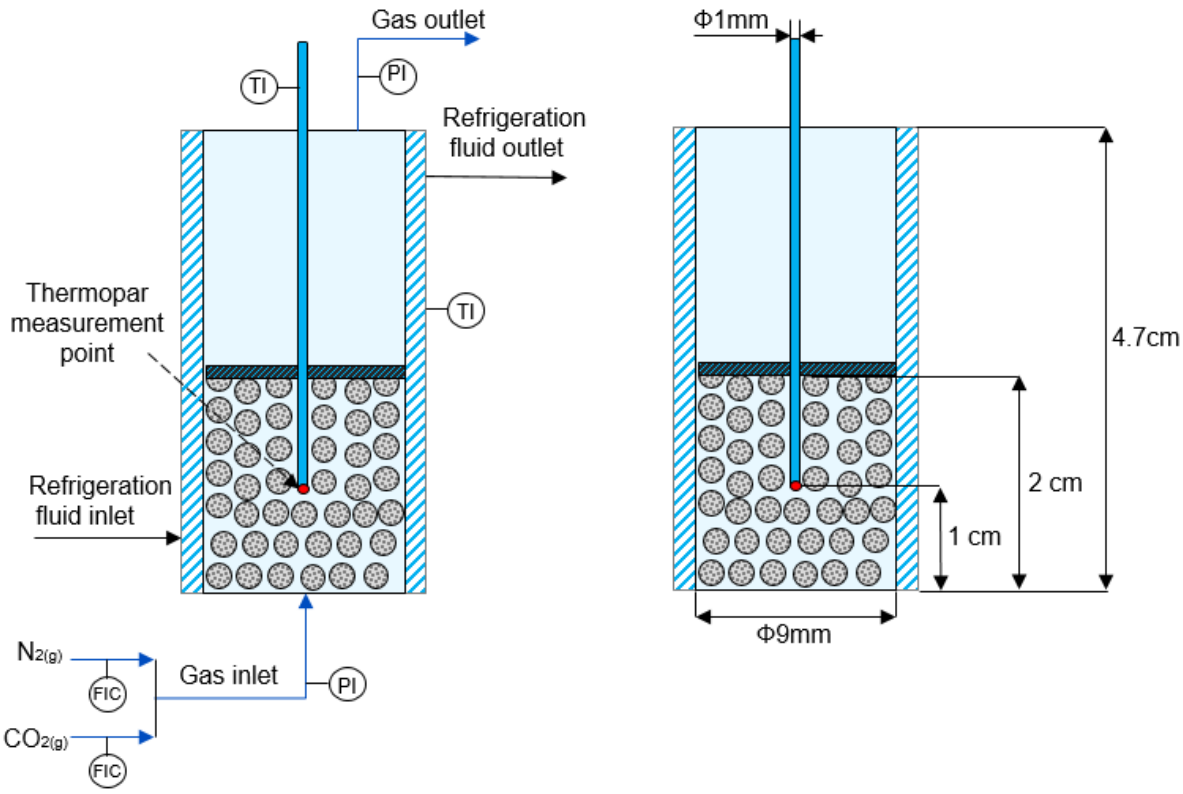

Figure 5. Simplified description of fixed-bed.

The valves to control the entrance of the flow where activated manually by a LabVIEW-based control environment. The temperature sensors were located in the gas inlet, gas outlet, jacketed and inside if the fixed-bed. The mass of the samples was 0.543 g of amine-resin, 0.786 g of Zeolite 13X and 0.887 g of Zeolite 4Å with a temperature prove in the middle. The conditions of the DAC adsorption in the fixed-bed are presented at **Table 3**, where the temperatures are referred to the temperature in the middle point of the fixed-bed.

Table 3. DAC experimental conditions for fixed-bed.

	T_{Ads} (ºC)	T_{Des} (ºC)	P_{Ads} (bar)	P_{Des} (bar)	$\dot{V}_{Ads}$(L(STP)/min)	$\dot{V}_{Des}$(L(STP)/min)	$CO_{2\ inlet}$ (ppm)
Amine-resin	25	100	1.1	1.1	1	1	400
	25	60-100	1.1	1.1	1	1	400
	25	60-100	1.1	1.1	1	1	400
	25	60-100	1.1	1.1	1	1	400
Zeolite 4Å (pellet)	25	100	1.1	1.1	1	1	400
	25	60-100	1.1	1.1	1	1	400
	0	100	1.1	1.1	1	1	400
	0	25-100	1.1	1.1	1	1	400
Zeolite 13X	25	100	1.1	1.1	1	1	400
	25	60-100	1.1	1.1	1	1	400

4.4 Determination of kinetic constants

Based in the experimental models found in bibliography and the reported results, the experimental LDF fitting models selected for this thesis study were LDF1, LDF2, Avrami and Veneman-LDF1. In addition, the LDF theoretical models selected were Farooq and Ruthven and Perry's model. After studied the options it was concluded that the calculus of the kinetic parameters using the LDF from the experimental data will produce an apparent constant. In this contest, apparent constant englobes all the mechanism of mass transfer during the adsorption, but the characteristic design parameters from the device would be included too such as concentration of adsorbate in the inlet, T, P and voidage. Thus, the apparent constant would be able to predict only the experiments carried out with the same device and same experimental conditions. However, the apparent kinetic constant will not be able to be used for the scale up of the process. On the other hand, the analytical determination is able to separate the contributions of the experiment conditions and design parameters to the adsorption kinetic constant. Thus, applying to the adsorption kinetic constant the new experiment conditions, a new approximation of the kinetic constant will appear being able to predict the behaviour of the new experiment. However, the second option would be able to predict the scale up of the process. In this thesis, both methods were studied, and the results will be discussed in the results section.

In order to be able to apply the kinetic adsorption models selected some assumptions were done. Assuming the isothermal trace system is a common assumption in DAC (Shafeeyan, Wan Daud, and Shamiri 2014). It is valid at very low concentrations of the adsorbate and it considers the variation in the heat of adsorption and the fluid velocity negligible (Shafeeyan, Wan Daud, and Shamiri 2014). This method was used by Buijs and De Flart (2017) to model the capturing process of CO_2 in a Fixed bed with amine based adsorbents. As result the mass transfer balance at fixed-bed used in this thesis is presented in (Eq. 36).

$$-D_L \frac{\partial^2 C}{\partial z^2} + u\frac{\partial C}{\partial z^2} + \frac{\partial C}{\partial t} + \left(\frac{1-\varepsilon}{\varepsilon}\right)\rho_p \frac{\overline{\partial q}}{\partial t} = 0; \qquad \text{(Eq. 36)}$$

Based on the information presented by Shafeeyan, Wan Daud, and Shamiri (2014), the equilibrium adsorption capacity selected for this thesis is the final value of the capacity at the equilibrium. In this thesis was decided to use a "black box model" for the calculus of the apparent constant, in which the boundaries in the equations where for L=L. In addition, the assumption of Zero-D kinetic model for adsorption was taken. Perry's model proposed for amine-resin assumes that the limitation step in the mass transfer was the pore diffusion based in the bibliography available. In addition, the N_2 adsorption in the solid is considered negligible. For the model of Farooq and Ruthven the diffusion coefficient for the macropore and micropore diffusion was assumed the combination of Knudsen and viscous flow. In addition, modifications were made to the (Eq. 32) in order to refer the capacity to the solid phase. The (Eq. 32) modified is presented at (Eq. 37).

$$\frac{1}{k_i} = \frac{R_p q_0 \rho_B}{3k_f c_0(1-\varepsilon)} + \frac{R_p^2 q_0 \rho_B}{15\varepsilon_p D_p c_0(1-\varepsilon)} + \frac{r_p^2}{15D_p} \qquad \text{(Eq. 37)}$$

The modelling conditions for the determination of diffusivity coefficients and adsorption kinetic constants are presented at **Table 4**.

Table 4. Modelling conditions for the calculation of the adsorption kinetic model constants.

Pressure (bar)	1.1
Temperature (K)	298
CO2 Concentration inlet (ppm)	400
Gas Flow rate inlet (L(STP)/min)	1
q_e Isotherm (mol/kg)	0.5445
q_e Experimental (mol/kg)	0.5562

5 RESULTS AND DISCUSSION

Firstly, the properties and characteristics from the adsorbent for the adsorption test will be introduced. In second place, the adsorbent characterization results such as particle porosity and particle density will be used to complete the capacity determination tool from (Elfving et al. 2017). The adsorption capacity results from the different test carried out will be compared and discussed. In addition, the viability of the Zeolites as adsorbent for DAC will be discussed in base to the capacity data obtained from fixed-bed and TGA. The adsorbent characterization results for the adsorbents and experimental conditions will be used to determine the kinetic modelling parameters. The kinetic modelling parameters such as the diffusion coefficients for Fickian model and the kinetic adsorption constants for the models based in LDF will be discussed. From the adsorption kinetics models comparison, the best kinetic model will be proposed for the amine-resin.

5.1 Characterization of the Adsorbents

5.1.1 Humidity test

The humidity test results carried out at LUT are presented at **Table 5**. The objective of the humidity test was to be able to determine the amount of moisture in the raw samples in order to consider it for the capacity correction.

Table 5. Humidity test for the studied adsorbents.

	Amine-resin	Zeolite 13X	Zeolite 4Å
M crucible (mg)	37654.6	38440.4	39843.8
M crucible + sample (mg) wet	38662.1	39442.5	40845.2
M crucible + sample (mg) dry	38655.4	39575.5	41005.5
% Moisture in sample	0.6650	-13.2721	-16.0076

From **Table 5** the high hydrophilic behavior is observed for zeolites tested. Thus, the zeolites did not lose any water in the desiccator, in fact Zeolite 13X gained a 13% of water and the Zeolite 4Å (pellets) a 16% in comparison with the wet sample. Therefore, the pretreatment was discarded for the zeolite samples.

5.1.2 Bulk, particle and skeletal densities

The results of particle and skeletal density for amine resin, Zeolite 4Å (Pellet) and Zeolite 4Å (Powder) obtained from the mercury pycnometry are presented in **Table 6**. On the other hand, the value of the skeletal and particle density for Zeolite 13X were taken from the study of Zarghampoor et al. (2017).

Table 6. Densities for the studied adsorbing materials.

Sample	ρ_s, skeletal density (kg/m3)	ρ_p, particle density (kg/m3)	ρ_b, bulk density (kg/m3)	Reference
Amine-resin	1024.60	696.73	448.89	-
Zeolite 13X	1952.38	1230.00	650.00	Zarghampoor et al. (2017)
Zeolite 4Å(pellet)	1131.70	888.38	732.40	-
Zeolite 4Å(powder)	540.10	370.21	370.20	-
Amine-resin /wet	827.70	559.30	448.89	-
Zeolite 4Å(pellet)/ wet	1478.40	1217.80	732.40	-
Zeolite 4Å(powder)/ wet	873.90	470.20	370.20	-

5.1.3 Adsorbents Porosity and Tortuosity

The results solid porosity and tortuosity for amine-resin, Zeolite 4Å (Pellet) and Zeolite 4Å (Powder) obtained from the mercury pycnometry are presented in **Table 7**. On the other hand, the value of the solid porosity and tortuosity for Zeolite 13X were taken from the study of Zarghampoor et al. (2017).

Table 7. Adsorbents Porosity and Tortuosity.

Sample	Ɛp, porosity	τ, Tortuosity factor	Reference
Amine-resin	0.3060	2.133	-
Zeolite 13X	0.3700	2.100	Zarghampoor et al. (2017)
Zeolite 4Å(pellet)	0.2147	0.016	-
Zeolite 4Å(powder)	0.3145	2.038	-
Amine-resin/wet	0.3243	2.099	-
Zeolite 4Å(pellet)/wet	0.1763	0.019	-
Zeolite 4Å(powder)/wet	0.461921	2.008	-

From **Table 7** is observed the differences in the internal structure of the adsorbents dried in comparison with the same samples with moisture.

5.1.4 Voidage

The voidage results volume for a bed of amine-resin particles for the adsorption and desorption temperatures is presented at the **Table 8**. In addition, one test without pre-regeneration (NR) was carried out in order to determine how the adsorbate adsorbed affect to the voidage volume.

Table 8. Amine-resin voidage results.

	25C				100C			
	NR	test 2	test 3	Average	NR	test 2	test 3	Average
ε_m	0.5199	0.5416	0.5379	0.5397	0.4251	0.4351	0.4466	0.4356
$uo_{,mf}$ (m/s)	0.1499	0.1858	0.1793	0.1826	0.0572	0.0635	0.0715	0.0641
$\dot{V}_{,m}$ (L/min)	0.5721	0.7094	0.6842	0.6968	0.2182	0.2423	0.2731	0.2445
$R_{ep,mf}$	5.8125	7.2069	6.9515	7.0792	2.2170	2.4621	2.7743	2.4845

The voidage average calculated from the experiments in the fixed-bed is similar to value obtained from the bulk and skeletal density, 0.5601. The void volume fraction in the bed was reduced by the increase of the temperature from 25 ºC to 100 ºC. Thus, the thermal dilatation of the particles should be taken in account to do a more accurate simulation of the desorption process.

5.2 Capacity

In this subchapter, the results of adsorption/desorption capacity will be presented and discussed. Additionally, the comparison of different adsorption and desorption temperatures tested will be presented. The model of Toth was selected for the calculus of the equilibrium capacity in this thesis. The decision was based in the study of Elfving, Bajamundi, and Kauppinen (2017) and Elfving (2015) in which was showed Toth model as the most accurate model in order to predict the adsorption of CO_2 for the amine-resin. In addition, Toth model was proposed too for the adsorption of CO_2 with the zeolites studied by Zarghampoor et al. (2017).

5.2.1 Fixed-bed results

The TSA adsorption results for the samples carried out in the fixed-bed are presented in the **Table 9**. All the materials were regenerated with pure nitrogen at 100ºC before and after

each experiment. At **Table 9** is included a comparison between the total desorption capacity obtained at 100 ºC and the desorption capacity obtained for intermediate temperatures such as 25 ºC and 60 ºC.

Table 9. Detailed equilibrium capacity (mol CO_2/ kg adsorbent) of adsorption and desorption results from fixed-bed for different temperatures.

		Adsorption		Desorption			
Temperature	Cycle	0 ºC	25ºC	25ºC	60ºC	100 ºC	$\dot{V}_{Ads}$ & $\dot{V}_{Des}$ set point (L(STP)/min)
Amine-resin	1	-	0.5562	-	-	0.5564	1
	2	-	0.5841	-	0.4966	0.5859	1
	3	-	0.5974	-	0.4944	0.5805	1
	4	-	0.5340	-	0.4871	0.5838	1
Zeolite 4Å (Pellet)	1	-	0.1357	-	-	0.1329	1
	2	-	0.1363	-	0.1010	0.1207	1
	3	0.1634	-	-	-	0.1534	1
	4	0.1195	-	0.0309	-	0.1004	1
Zeolite 13X	1	-	0.1532	-	-	0.1074	1
	2	-	0.0698	-	0.0480	0.0679	1
	3	0.0872	-	0.0600	-	0.0905	1
	4	0.1307	-	-	-	0.1166	1
	5	-	0.0320	-	-	0.0543	2

Based in the fixed-bed capacity results in the **Table 9**, amine-resin showed stability for different conditions of desorption after the 4 cycles and the desorption process in two steps (first 60ºC and after 100ºC) did not showed bid differences in the total desorption capacity. Additionally, the desorption at 60 ºC removed the 84% of the total CO_2 desorbed at 100ºC. Thus, decreasing the desorption temperature to 60ºC could decrease the operational cost of the process. The small differences in the capacity as result of the measurement sensor of CO_2 needed to be recalibrated.

Zeolites adsorption capacity improved for adsorption temperatures under 0ºC. The result confirms the assumption of the CO_2 adsorption in zeolites is controlled by the thermodynamic of the process. The adsorption is an exothermal process and it is favoured by low temperatures. Zeolite 4Å showed stability during the three-initial test, loosing partially the adsorption capacity at the fourth test. The low temperature of 0 ºC increased the adsorption capacity in a 20% in comparison with 25ºC. In addition, the temperature effect in desorption showed that at 60ºC was removed an 84% of the total CO_2 desorbed at 100ºC.

Zeolite 13X showed an adsorption capacity elevated for a physisorbent in comparison other physisorbents following the trend found by Siriwardane et al. (2001). In addition, Siriwardane et al. (2001) concluded that the elevated capacity was result of the sieve effect for zeolites with small porous. In addition the results follow the trend found by Siriwardane et al. (2001), who proposed the Zeolite 13X as separation material for N_2/CO_2 mixes. The reduction in the adsorption capacity after one cycle was drastic (50%) compared with the adsorption capacity of the fresh sample. Thus, the reduction in the capacity indicated that the regeneration step was not enough to remove completely the CO_2 adsorbed by the zeolite. The results in the reduction of capacity for CO_2 adsorption on Zeolite 13X were reported by Konduru et al. (2015), who used as regeneration step helium at 135ºC. In addition, the study of Siriwardane et al. (2001) showed a completely regenerability for the Zeolite 13X in CO_2 adsorption, after elevate the temperature of the regeneration step to 250ºC. Besides the reduction found for the test 2, during test 3 the lower adsorption temperature showed an increase in the adsorption capacity in comparison with the test 2. In addition, desorption in the test 3 showed a value higher than the adsorbed, which could be explained as the desorption step started to drag the trapped molecules by the molecular sieve. The drag process is referred to CO_2 physically removed by the effect of the fluid flow crossing the pores. The trap effect is referred to the particles of CO_2 that could not be removed during the regeneration step. As result of the drag effect, part of the adsorption capacity was recovery as it was shown in the test 4. In the test 4 the partially regenerated zeolite showed adsorption capacity again, but the desorption capacity showed that the “trap effect” of the adsorbent in the zeolite started again. From the last test cannot be obtained any conclusion because the zeolite was not regenerated totally. As consequence of the fast reduction of the adsorption capacity and the limitations in the regenerability showed during the fixed-bed experiments, the Zeolite 1 was considered not interesting for DAC technologies under the conditions tested.

The **Figure 6** shows a graphical comparison of the adsorption capacity curves from the different amine-resin cycles presented at **Table 9**.

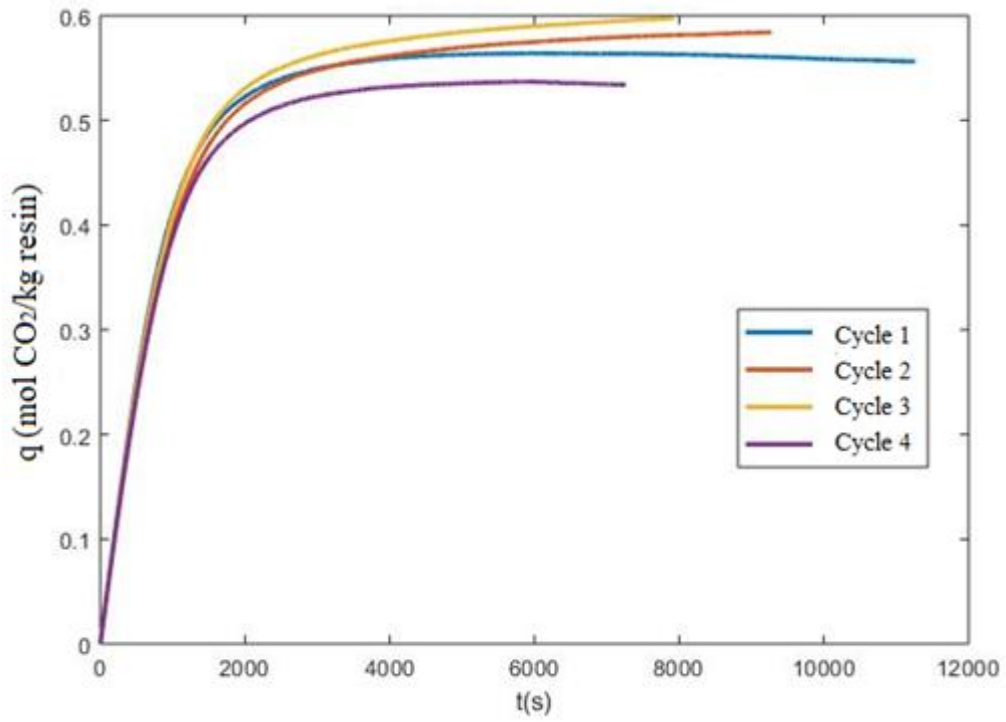

Figure 6. Amine-resin adsorption capacity from fixed-bed experiments.

From the **Figure 6** can be observed that all the curves follow the same behaviour in linear capacity region for time < 1000 seconds. Based in the (Eq. 27) the apparent adsorption kinetic constant for the LDF is the slope of the capacity curve. Thus, the apparent adsorption kinetic constant coincided between experiments.

The **Figure 7** shows a graphical comparison of the adsorption capacity curves from the different cycles of adsorption from Zeolite 4Å and Zeolite 13X fixed-bed tests presented at **Table 9**.

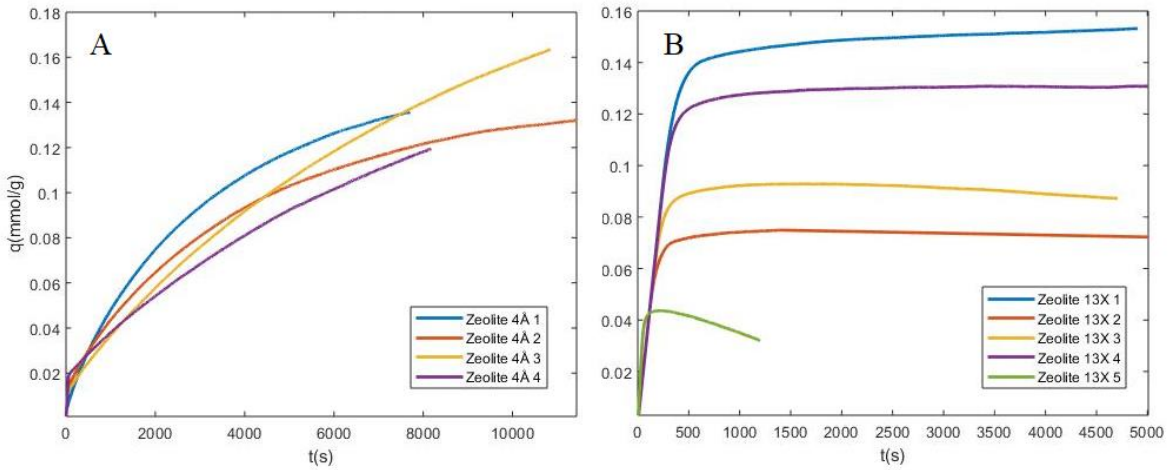

Figure 7. Zeolites adsorption capacity from fixed-bed experiments. A corresponds to Zeolite 4Å capacity. B corresponds to Zeolite 13X capacity.

From the **Figure 7 A** is observed that apparently the behaviour for the adsorption step at 25ºC differed from cycle 1 to cycle 2. However in the Appendix II is included a zoom of **Figure 7** A in which is observed that the linear behaviour for Zeolite 4Å was presented for a time below 60 seconds. In the **Figure 7 B** the linear behaviour of Zeolite 13X is presented by time below 250 seconds. In the Appendix II is included a zoom of the linear trend for Zeolite 13X.

5.2.2 TGA results

The adsorption equilibrium capacity results for the dry and wet samples carried out in TGA are presented at **Table 10**.

Table 10. TGA equilibrium capacity results. Wet adsorbent term is referred at the supplied adsorbent without any pre-treatment.

		Sample mass (mg)	$q_{e,Ads}$ (mol/kg)	$q_{e,Des}$ (mol/kg)	$q_{e,only\ CO2}$ (mol/kg)	$q_{e\ H2O}$ (mol/kg)
Amine-resin	dry	5.90	0.5232*	0.6550	-	-
	wet	6.46	0.5030	0.7041	0.5475	0.1566
	dry	10.26	0.5581	0.6151	-	-
	wet	10.47	0.5270	0.6913	0.5307	0.1605
Zeolite 4Å (Pellet)	dry	30.95	0.4415	0.3168	-	-
Zeolite 13X	dry	5.66	1.6907	1.4464	-	-

The comparison between the dry samples and the wet samples showed that the capacity of adsorption for the wet samples in a little lower than the dry samples as it can be observed from **Table 10**. In addition, increasing the mass sample the equilibrium adsorption capacity increased. However, based in the geometry of the TGA sample cup and the sensibility of the balance, increasing the sample mass the contribution of the measurement error was reduced. The presence of the moisture in the samples increased the mass transfer resistance for CO_2, and as a result the amount of CO_2 that was able to react with the amine was lower in comparison with a dry sample. Thus, the lower amount of CO_2 fixed by the resin explained the lower equilibrium capacity in comparison with a dry sample. TGA resin samples showed an equilibrium capacity close to the value found for the fixed-bed experiments. In addition the adsorption equilibrium capacity for the amine-resin calculated with isotherm from Elfving (2017) was 0.5445. As conclusion, TGA and fixed-bed are able to obtain the similar equilibrium capacity values for the dry amine-resin. In addition, both methods showed adsorption capacity values close to value from the isotherm with a maximum deviation of 4% for TGA dry samples and a 9% for fixed-bed.

Zeolites results from TGA experiments apparently differed with the results from fixed-bed. The humidity test carried out showed that the standardized method in LUT used for drying the samples was not able to ensure the water removing from the zeolite samples. In addition, the humidity test showed that zeolite samples gained weight after the drying process. As conclusion, zeolites showed a more hydrophilic behaviour than the lab desiccator and as a result the zeolites samples gained humidity during the drying process. Thus, the results of the zeolites adsorption capacity could have been affected by the presence of moisture in the samples. In addition, the equilibrium capacity for both zeolites samples was still increasing when the adsorption step ended (12h). In the studies of Park et al. (2016) & Garshasbi, Jahangiri, and Anbia (2017) of CO_2 adsorption capacity on Zeolite 13X, the CO_2 adsorption capacity obtained was 1.581 mol/kg for 1810 Pa of pure CO_2 at 293K. Thus, the 44 Pa of CO_2 diluted and 298K used in the TGA adsorption capacity are not able to explain the capacity registered by the TGA in base to the concentration of CO_2 used in the zeolite experiments.

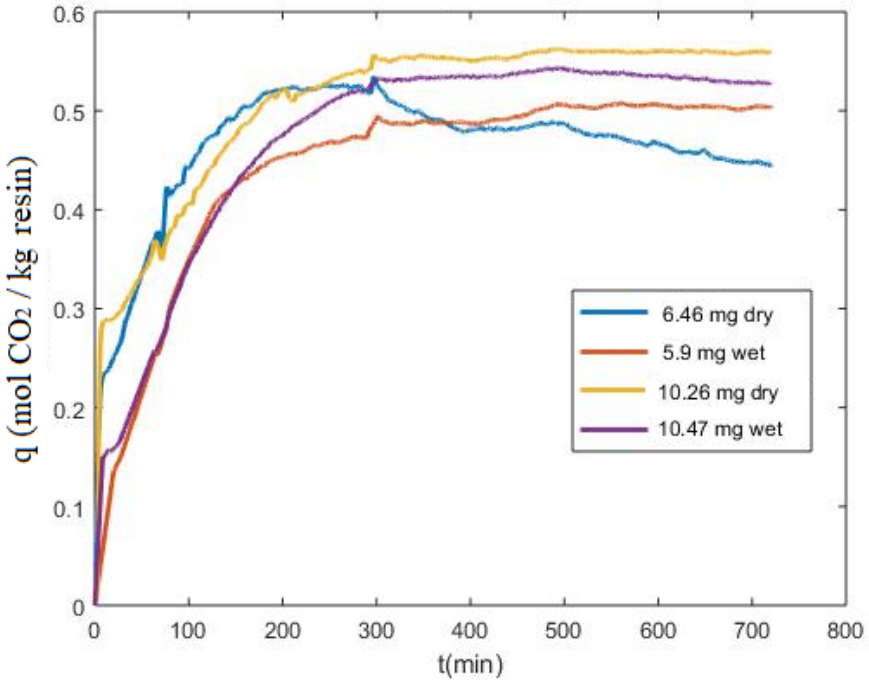

Figure 8. TGA adsorption capacity results.

6.46 mg dry amine-resin sample showed a stable capacity value 0.5232 (mol/kg) for 100 min and after it decreased until 0.4432 (mol/kg) presented in **Figure 8**. The change in the equilibrium capacity can be explained as during the adsorption process an external perturbation in the system happened such as CO_2 concentration decreased in the TGA inlet. The perturbation explanation makes sense if the value of the capacity is compared with the equilibrium capacity results obtained for the amine-resin in this work or with the value of adsorption capacity isotherm, 0.5445 (mol/kg).

TGA samples needed time to achieve the equilibrium capacity almost 10 times longer than the fixed-bed samples. The high difference in the time of equilibrium is explained by the differences in the phase contact between the gas and the solid, the flow rate and the diffusion coefficient. The flow crossing the fixed-bed has better contact between the solid surface and the gas, as consequence the resistance to the mass transfer and concentration of CO_2 available close to the surface is higher.

5.3 Kinetic models

In this section, the different models for Kinetics of Adsorption studied will be compared under same representative conditions of temperature, CO_2 concentration and pressure of a DAC process. In addition, the validity of the models for the determination of adsorption kinetics constants will be discussed.

5.3.1 Diffusivity coefficients determination

The determination of the diffusivity coefficients was a fundamental step in the calculation of the kinetic models studied in this thesis. The dominant diffusion coefficients presented in this chapter are the diffusivity coefficient used in the Fickian model (Eq. 1). In addition, the diffusivity coefficients were used in the theoretical adsorption kinetic constant determination. In this chapter, the results obtained for the diffusion coefficients for the fixed-bed and TGA experiments will be presented. The conditions used for the calculations of the diffusivity coefficients are presented at **Table 11**.

Table 11. Conditions for the diffusivity coefficients.

Pressure (bar)	1.1
Temperature (K)	298
CO_2 Concentration (%)	0.04
Concentration of N_2 (%)	0.96
Gas Flow rate fixed-bed (L(STP)/min)	1
Gas Flow rate TGA (mL(STP)/min)	50

In **Table 12** are presented the fixed-bed and TGA diffusion coefficients for the Fickian model descripted in (Eq. 1) from the amine-resin samples.

Table 12. Amine-resin diffusion coefficients for the fixed-bed and TGA experiments. The (Eq. 24 proposed by Wakao and Funazkri it valid for gas or liquid with $3 < Re_p < 10^4$, as consequence of the low flow used in the TGA the Rep is 2.7. Thus, Sh was calculated from the approximation proposed by Carberry available in Perry et al. (1999) presented at (Eq. 24*, which is valid for gas or liquid with $Re_p > 1$.

Diffusion coefficients		**Fixed-bed**	**TGA**	**Equation**
$D_{m,ef\ CO2/N2}$	m^2/s	2.17E-06	2.17E-06	(Eq. 7)

$D_{k,ef\ CO2}$	m^2/s	2.79E-07	2.79E-07	(Eq. 10)
$D_{k,ef\ N2}$	m^2/s	3.50E-07	3.50E-07	(Eq. 10)
$D_{v,ef}$	m^2/s	1.54E-05	1.54E-05	(Eq. 18)
K_n	-	2.84	2.84	(Eq. 13)
D_{eff} (Knud+mol))	m^2/s	2.48E-07	2.48E-07	(Eq. 16)
D_{eff} (Knud+vis)	m^2/s	2.75E-07	2.74E-07	(Eq. 16)
k_f	m/s	0.13	0.06	(Eq. 24)*
D_L	m^2/s	6.74E-04	-	(Eq. 25)

$$Sh = \frac{2k_f R_p}{D_m} = 1.1\left(\frac{Re_p}{\varepsilon}\right)^{0.5} Sc^{0,33} \qquad \text{(Eq. 24)*}$$

From **Table 12** can be observed that Knudsen number obtained for the gas composition in the inlet is 2.84. Thus, the Knudsen number is below 10 and as a result the diffusion process is a combination of Knudsen and viscous flow as was explained in the chapter 2.1 and according with the studies of Bos et al. (2018). In addition, combination of Knudsen and molecular diffusion was calculated in order to compare the differences with the combination of Knudsen and Viscous flow. Additionally, the comparison did not show important differences in the value of the diffusion coefficient. Comparing the column from fixed-bed and TGA it can be observed that the only parameter that changed is the external diffusion coefficient k_f. As it will be discuss in the subchapter 5.3.3, experimentally was found that the prognosis for the TGA diffusivity coefficient included in **Table 12** was not able to predict the behaviour of the TGA. The difference is created by a counter diffusivity flow originated by the geometry of the TGA crucible (Pérez and Ariso 2008). Therefore, the diluted CO_2 flow finds in its way to contact the adsorbent an additional resistance originated by the non-adsorbed N_2 flow trying to get out of the crucible. The counter diffusion effect has been described in literature for authors such as Ruthven (1984) & Do (1998). In order to obtain a diffusivity coefficient able to predict that behaviour the method of Farooq and Ruthven-LDF was compared with the LDF1 apparent kinetic constant. Solver Excel tool was used to determine the corrected diffusivity coefficient for the TGA experiments presented in Table 13. In addition, the diffusivity coefficient for the TGA experiments with moisture was calculated and it is included in the **Table 13**.

Table 13. Corrected amine-resin diffusion coefficients for the TGA experiments.

Diffusion coefficients TGA		
$D_{ef\ CO_2}$ (TGA, dry)	m2/s	5.52E-08
$D_{ef\ CO_2}$ (TGA, wet))	m2/s	3.29E-08
k_f	m/s	6.22E-02

From **Table 13** is observed that the diffusivity coefficient for the samples with moisture was lower than for dry samples. The lower diffusivity coefficient for the samples with moisture effect was a combination between the changes in the physical properties of the adsorbent such as tortuosity and the interference of the water in CO2 adsorption process.

The results of the calculations of the diffusion coefficients for the Zeolite 13X are presented at **Table 14**.

Table 14. Zeolite 13X diffusion coefficients for the fixed-bed experiments.

Diffusion coefficients fixed-bed			**Equation**
$D_{mef\ CO_2/\ N_2}$	m^2/s	2.52E-06	(Eq. 7)
$D_{kef\ CO_2}$	m^2/s	2.89E-08	(Eq. 10)
$D_{kef\ N_2}$	m^2/s	3.62E-08	(Eq. 10)
D_{vef}	m^2/s	1.43E-07	(Eq. 18)
K_n	-	3.17E+01	(Eq. 13)
k_f	m/s	1.57E-01	(Eq. 24)*
D_L	m^2/s	7.24E-04	(Eq. 25)

From **Table 14** can be observe that Knudsen number is elevated (>10) and as result the diffusion was dominated by the Knudsen flow (Do 1998). Thus, the elevated Knudsen number implied that the Diffusion coefficient is equal to the Knudsen Diffusion Coefficient ($Dk_{ef\ CO_2}$). In addition, the big difference between the Knudsen Diffusion Coefficient for N_2 and CO_2 explained the elevated adsorption capacity in comparison with other physisorbents.

The results of the calculations of the diffusion coefficients for the Zeolite 4Å (Pellets) are presented at **Table 15**.

Table 15. Zeolite 4Å (Pellets) diffusion coefficients for the fixed-bed experiments.

Diffusion coefficients fixed-bed			**Equation**
$D_{mef\ CO_2/\ N_2}$	m2/s	2.08E-04	(Eq. 7)
$D_{kef\ CO_2}$	m2/s	6.79E-07	((Eq. 10)

$D_{kef\ N2}$	m2/s	8.51E-07	(Eq. 10)
D_{vef}	m2/s	1.03E-06	(Eq. 18)
K_n	-	103.08	(Eq. 13)
k_f	m/s	8.80E-02	(Eq. 24)*
D_L	m2/s	4.79E-03	(Eq. 25)

The elevated Knudsen number of 103.00 presented in **Table 15** indicated the dominance of Knudsen diffusion and as result the diffusion coefficient for the conditions studied was Knudsen Diffusion Coefficient.

During the experimental planning, Zeolite 4Å (Powder) was excluded from the experiments because of possible problems that could be caused by the small particle size of the sample zeolite. Besides of the exclusion of the Zeolite 4Å (Powder) in the experimental phase, theoretical calculations included in **Table 16** were done in order to supply the necessary information for future experiments.

Table 16. Zeolite 4Å (Powder) diffusion coefficients for the fixed-bed experiments.

Diffusion coefficients fixed-bed			**Equation**
$D_{mef\ CO2/\ N2}$	m2/s	2.39E-06	(Eq. 7)
$D_{kef\ CO2}$	m2/s	7.79E-09	((Eq. 10)
$D_{kef\ N2}$	m2/s	9.77E-09	(Eq. 10)
D_{vef}	m2/s	1.19E-08	(Eq. 18)
K_n	-	1.03E+02	(Eq. 13)
k_f	m/s	4.71E+01	(Eq. 24)*
D_L	m2/s	10.51	(Eq. 25)

The elevated Knudsen number of 103.00 presented at **Table 16** indicated the dominance of Knudsen diffusion and as result the diffusion coefficient for the conditions studied was Knudsen Diffusion Coefficient. In addition, the comparison of **Table 15** and **Table 16** confirmed that particle characteristics such as the particle size affect the diffusion in the adsorbent of CO_2. An example of the dependence of the diffusion coefficients of the solid characteristics can be observed in the value of the $Dk_{ef\ CO2}$ which value is of 6.78E-07 for the Zeolite 4Å (pellets) and 7.79E-09 for the Zeolite 4Å (powder). In addition, the high value of the axial dispersion for the Zeolite 4Å (powder) was interpreted as the zeolite could create operation problems in fixed-bed. Thus, the zeolite 4Å was not included in the capacity experiments.

5.3.2 Fixed-bed CO_2 LDF Adsorption Kinetic Models

In this subchapter are included the results of the adsorption kinetic models proposed at the operation conditions included in the **Table 4**. The experimental capacity curve chosen as experimental equilibrium capacity is presented in the **Figure 6** as "cycle 1" and it correspond to the first raw of **Table 9**. In addition, as all the curves had the same slope, whatever of the other cycles could be chosen to determine the apparent constant. The adsorption kinetic constants from Farooq and Ruthven model (Eq. 37) are presented at **Table 17**:

Table 17. Farooq and Ruthven Model results for fixed-bed.

qe source	External Diffusion Resistance (s)	Macropore Diffusion Resistance (s)	Micropore Diffusion Resistance (s)	Overall Resistance, 1/k (s)	Farooq and Ruthven-LDF, k (s^{-1})
Experiment	24.7250	690.0100	1.32E-11	714.7300	1.40E-03
Isotherm	24.2040	675.4900	1.32E-11	699.7000	1.43E-03

The results from the model of Farooq and Ruthven showed that the contribution of the micropore diffusion was insignificant and dominant resistance was located in the macropore diffusion. In addition, the macropore diffusion coefficient was considered the combination of Knudsen and viscous flow diffusion as it was showed in the chapter 5.3.1.

The adsorption kinetic coefficients for Perry's model (Eq. 32) at fixed-bed conditions is presented at **Table 18**.

Table 18. Perry Model determination for fixed-bed.

Coefficients and units		Experimental	Isotherm
ε_{mf}	-	0.5397	0.5397
ε_p	-	0.3100	0.3100
τ	-	2.1000	2.1000
ρ_b	kg/m3	448.8850	448.8850
C_{iref}	mol/m3	0.0178	0.0178
n_{iref}	mol CO2 ads/kg ads	0.5562	0.5445
C_b	mol/m3	44.3796	44.3796
n_{iB}	mol N2 ads/kg ads	-	-
Λ	-	14058.8319	13763.0960
R	-	0.0144	0.0144
Ψ_p	-	0.7750	0.7750
k_n	s-1, Perry's constant	1.12E-03	1.15E-03

The apparent adsorption constants were determined fitting the shape of the amine-resin adsorption capacity results curve to the models programmed in Matlab. A fitting tool was used to adjust the apparent adsorption kinetic constant to the capacity curve similar to (Elfving et al. 2017). The pertinent changes adapted the tool to the fixed-bed and TGA scenarios studied in this thesis. As result of the changes, the code nowadays is able to determine the constants for the models found in **Table 19** and **Table 22.** For the theoretical methods an Excel file was developed including the properly calcules and the results are presented at **Table 19** and **Table 22**. The results were:

Table 19. Comparison of fixed-bed amine-resin adsorption kinetic constants.

		From isotherm	From experimental	Equation
Fitting models (apparent kinetic constant)	Pseudo-First order (LDF1)	1.40E-03	1.32E-03	(Eq. 27)
	Pseudo-Second order (LDF2)	7.18E-03	6.21E-03	(Eq. 28)
	Avrami	1.49E-03; n=1.1	1.41E-03; n=1.1	(Eq. 29)
	Veneman-LDF	1.94E-03	1.98E-03	Rens Veneman et al. (2015 & 2016)
	Veneman–LDF f(X_{CO2})	3.18E+00	3.00E+00	(Eq. 30)
LDF theoretical methods	Farooq and Ruthven-LDF	1.47E-03	1.44E-03	(Eq. 37)
	Perry's LDF	1.18E-03	1.16E-03	(Eq. 32)

The results from the studied adsorption kinetic models included in the **Table 19** are presented in the **Figure 9**.

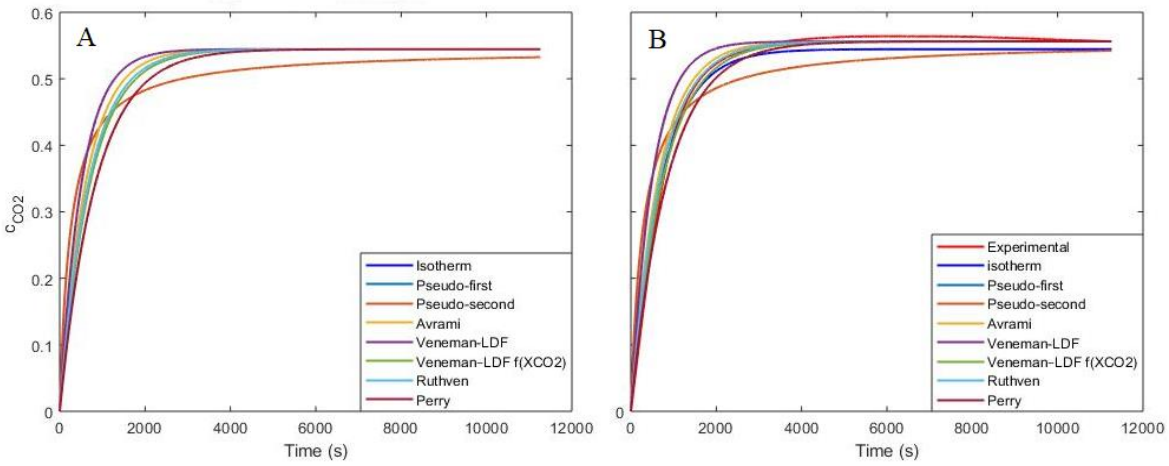

Figure 9. Adsorption Kinetic Model comparison. Graph A corresponds to the constants calculated from q_e isotherm. Graph B corresponds to the constants calculated from q_e experiments.

From **Figure 9 A** is observed that the best approximations for the experimental capacity curve are in order from the best to the worst accurate: Veneman LDF-f(X_{CO_2}) and LDF1 had totally match with the isotherm, Farooq and Ruthven-LDF, Avrami, Veneman-LDF and Perry. From **Figure 9 B** is observed that the best approximations for the experimental capacity curve are in order from the best to the worst accurate: the model of Farooq and Ruthven-LDF, the Veneman LDF-f(X_{CO_2}), LDF1 and Avrami, Perry's, Veneman-LDF and LDF2. The results validated the theoretical model proposed by Farooq and Ruthven as a good prediction for the adsorption kinetic constant of amine-resin. The model of Farooq and Ruthven-LDF for the Fixed-Bed conditions simulated assumed that the biggest contribution to the mass transfer resistance was in the pore diffusion (Farooq and Ruthven 1990). Thus, the validation of the model implies that the pore diffusion is the limiting step in the mass transfer diffusion.

5.3.3 TGA CO_2 LDF Adsorption Kinetic Models

As was explained in the chapter 5.2.2 the adsorption capacity profiles for the amine-resin samples at TGA needed ten times longer time to reach the equilibrium capacity. Initially the differences in the time where assumed as consequence of the differences in the flow rate in TGA in comparison with the Fixed-Bed experiments. Lately in the theoretical modelling of the TGA adsorption was observed that the differences in the flow rate where not able to predict the big differences in the apparent constants between the Fixed-Bed and TGA. The solution was found studying in more detail the geometry of the TGA adsorption sample cup. As result, it was observed that the diffusion coefficient used in Fixed-Bed was not the same that in TGA, as it was explained in more detail at chapter 5.3.1. Using the corrected diffusion coefficient from **Table 13**, the kinetic parameters used in the theoretical models were able to predict the adsorption behaviour at TGA. The coefficients for the theoretical models are presented at **Table 20** and **Table 21**.

Table 20. Farooq and Ruthven Model (Eq.37) results for TGA.

Sample	q_e source	External Diffusion Resistance (s)	Macropore Diffusion Resistance (s)	Micropore Diffusion Resistance (s)	Overall Resistance, 1/k (s)	Farooq and Ruthven-LDF k (s^{-1})
5.9 mg dry	Isotherm	48.10	3250.0	6.36E-11	3300.0	3.03E-04
	Experiment	46.20	3120.0	6.36E-11	3170.0	3.16E-04
6 mg wet	Isotherm	48.10	5450.0	1.07E-10	5500.0	1.82E-04
	Experiment	44.40	5030.0	1.07E-18	5080.0	1.97E-04
10.26 mg dry	Isotherm	48.10	3250.0	6.36E-11	3300.0	3.03E-04
	Experiment	49.30	3330.0	6.36E-11	3380.0	2.96E-04
10.47mg wet	Isotherm	48.10	5450.0	1.07E-10	5500.0	1.82E-04
	Experiment	46.60	5270.0	1.07E-18	5320.0	1.88E-04

Table 21. Perry Model (Eq. 32) determination for TGA.

Variable		5.9 mg dry		6 mg wet		10.26 mg dry		10.47mg wet	
		qe Iso	qe Exp	qe Iso	qe Exp	qe Iso	qe Exp	qe Iso	qe Exp
ε_{mf}	-	0.5397	0.5397	0.5397	0.5397	0.5397	0.5397	0.5397	0.5397
ε_p	-	0.3200	0.3200	0.3200	0.3200	0.3200	0.3200	0.3200	0.3200
τ		2.1000	2.1000	2.1000	2.1000	2.1000	2.1000	2.1000	2.1000
ρ_b	kg/m3	448.8850	448.8850	448.8850	448.8850	448.8850	448.8850	448.8850	448.8850
C_{iref}	mol/m3	0.0178	0.0178	0.0178	0.0178	0.0178	0.0178	0.0178	0.0178
n_{iref}	mol CO_2/kg ads	0.5445	0.5232	0.5445	0.5030	0.5445	0.5581	0.5445	0.5270
C_b	mol/m3	44.3796	44.3796	44.3796	44.3796	44.3796	44.3796	44.3796	44.3796
n_{iB}	mol N_2/kg ads	0	0	0	0	0	0	0	0
Λ	-	13763.0960	13224.7049	13763.0960	12714.1180	13763.0960	14106.8574	13763.0960	13320.7559
R	-	0.0165	0.0165	0.0179	0.0179	0.0143	0.0143	0.0162	0.0162
Ψ_p	-	0.7750	0.7750	0.7751	0.7751	0.7750	0.7750	0.7750	0.7750
k_n	Perry's constant, s-1	2.38E-04	2.48E-04	1.42E-04	1.54E-04	2.38E-04	2.33E-04	1.42E-04	1.47E-04

The overall of the CO_2 kinetic adsorption constants for TGA are presented at **Table 22**. In addition, at the same table can be observed the comparison of the adsorption kinetic constants for different sample mass and at moisture presence.

Table 22. Comparison of amine-resin adsorption TGA kinetic constants.

		Apparent kinetic constants				Theoretical kinetic constant	
Sample	q_e	LDF1	LDF2	Avrami (n=1.1)	Veneman f(XCO2)	Farooq and Ruthven LDF	Perry's LDF
5.9 mg dry	Isot	3.18E-04	1.41E-03	3.41E-04	7.23E-01	3.03E-04	2.33E-04
	Exp	3.62E-04	1.77E-03	3.86E-04	8.23E-01	3.16E-04	2.48E-04
6 mg wet	Isot	1.48E-04	5.95E-04	1.62E-04	3.36E-01	1.82E-04	1.42E-04
	Exp	1.94E-04	9.56E-04	2.08E-04	4.41E-01	1.97E-04	1.54E-04
10.26 mg dry	Isot	2.92E-04	1.64E-03	3.12E-04	6.64E-01	3.03E-04	2.39E-04
	Exp	2.66E-04	1.34E-03	2.85E-04	6.04E-01	2.96E-04	2.33E-04
10.47mg wet	Isot	1.74E-04	7.73E-04	1.86E-04	3.95E-01	1.82E-04	1.42E-04
	Exp	1.91E-04	9.38E-04	2.03E-04	4.34E-01	1.88E-04	1.47E-04
Equation	-	(Eq. 27)	(Eq. 28)	(Eq.29)	(Eq.30)	(Eq. 37)	(Eq. 32)

Note: Exp = Experimental equilibrium capacity; Iso = Isotherm equilibrium capacity.

Comparing the **Table 22** with **Table 19** it is observed that the apparent kinetic constant order for TGA was ten times smaller than for fixed-bed. In addition, differences in the comparison apparent kinetic constant from TGA and fixed-bed is explained by the own definition of apparent constant. An apparent kinetic constant is only able to explain the behaviour of the system studied under the same conditions and the same device. Thus, as the TGA and fixed-bed experiments were not carried out in the same device and with same flow rate, the results are different. The results from the studied adsorption kinetic models included in the **Table 22** are presented at **Figure 10**.

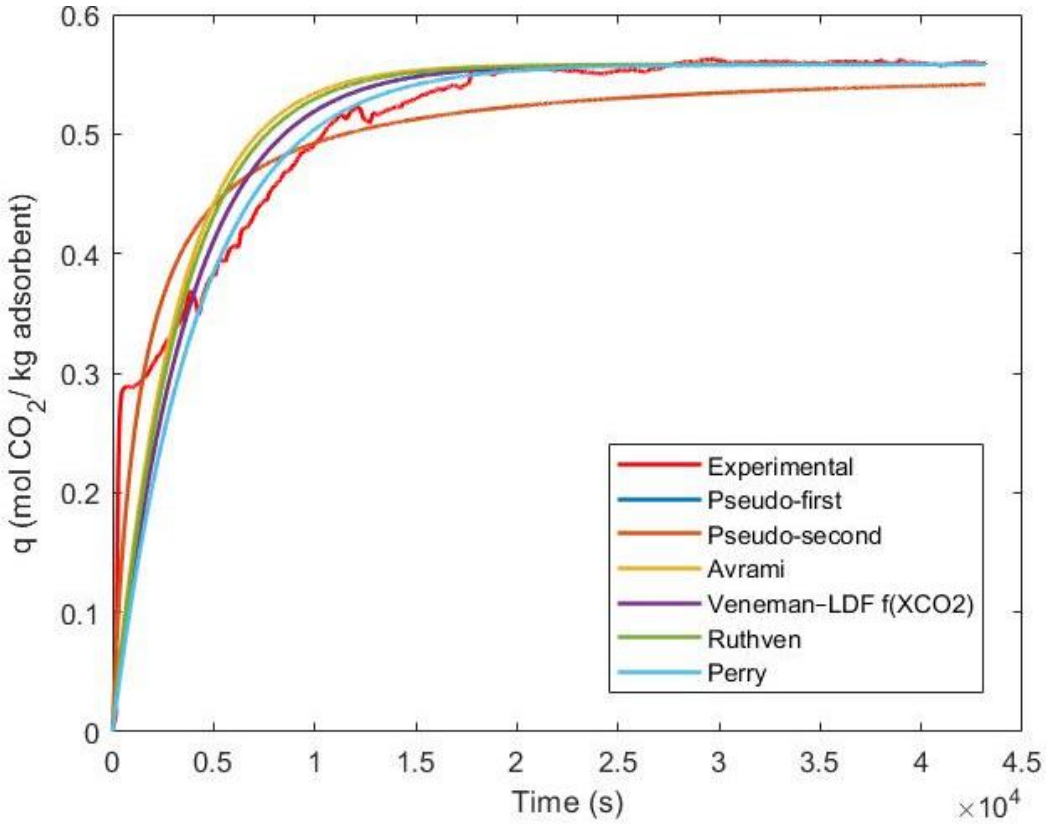

Figure 10. Adsorption Kinetic Model comparison. The graph corresponds to the constants calculated from q_e experiments, 10.26 mg dry sample.

From **Figure 10** is observed that the best approximations for the experimental capacity curve are in order from the best to the worst accurate: Perry's, Veneman LDF-f(X_{CO_2}), Farooq and Ruthven-LDF, Avrami, LDF1 and LDF2 in last position. However, except LDF2, all the methods converge to the experiment capacity at the same point.

6 CONCLUSIONS

Kinetic models based in LDF approximations are the most proposed approximations for the determination of CO_2 kinetic adsorption constants. LDF approximations for the CO_2 adsorption were able to predict the adsorption of CO_2 on the amine-resin samples. From the literature review it was concluded that the kinetic constants obtained directly from the fitting models to the experimental curves are apparent constants. In addition, the experimental fitting models generate an adsorption kinetic constant that englobes all the mass transfer resistances, but it does not quantify the contribution of each resistance to the global resistance. Thus, those methods are only able to predict the behaviour of the solid adsorbent for the same experimental conditions and characteristics of the device, and as a result their usefulness is limited. The best fitting model approximation for the amine-resin samples were LDF, Veneman LDF-f (X_{CO_2}) and Avrami. On the other hand, the theoretical determination methods quantify the contribution of each mass transfer resistance step. Thus, the kinetic adsorption constant for other conditions can be determined just changing the variables studied by the new process conditions and the adsorption device characteristics. The theoretical model of Farooq and Ruthven was found as an accurate estimation of the kinetic of adsorption for TGA and fixed-bed adsorption experiments. Therefore, the Zero-D kinetic adsorption assumption is a valid in the estimation of the kinetic adsorption constant. In addition, the results from the Farooq and Ruthven model showed that the limiting step in the adsorption of CO_2 on amine-resin is the pore diffusivity in the macropores. The positive results obtained from the modelling of the kinetic adsorption determination open the possibility to apply the modelling to other adsorbent materials, such as zeolites. Additionally, the coefficient of diffusion for the Fickian model were determined but the validation and simulation should be further studied.

The pore diffusion coefficient for amine-resin samples at the studied conditions was a combination of Knudsen and viscous flow diffusion. For the zeolite's samples, the Knudsen number indicated the dominance of the Knudsen flow in the pore diffusion coefficient. Comparing the equilibrium capacity results from TGA and fixed-bed was concluded that the mass transfer diffusion coefficient was not the same. Thus, TGA experiments showed and additional diffusion mass transfer resistance. The additional diffusivity mass transfer

resistance was included in the new calculation of the diffusion coefficients used for the adsorption kinetic constant determination from TGA. The corrected TGA diffusion coefficient explained the differences in the time necessary to achieve the adsorption equilibrium in comparison with fixed-bed. Fixed-bed and TGA showed values of equilibrium capacity for the amine-resin samples similar to the equilibrium capacity from the isotherm. Thus, both devices were considered valid for the equilibrium capacity determination.

The fixed-bed void volume determination showed the dependence of the void volume from temperature. As a result, more complex modelling for the mass transfer in amine-resin fixed-beds should include the bed porosity as temperature dependent variable.

The adsorption capacity behaviour for the studied amine-resin matched with the results found in literature. The amine-resin preserved the capacity after four adsorption-desorption cycles. Desorption at 60ºC removed 84% of the total CO_2 desorption at 100ºC. Thus, the profitability of the DAC processes could be improved by decreasing the desorption temperature from 100ºC to 60 ºC. TGA samples without pre-regeneration showed a lower capacity value as result of the lower value of the diffusion coefficient. The decrease indicates that the water needs to be supplied with the CO_2 in order to produce the formation of ammonium bicarbonate. Thus, the presence of the water in the raw sample only impedes that the CO_2 contact the amine and as a result the yield of the reaction of carbamate decreases.

Zeolite 4Å and Zeolite 13X were found possible future separation materials for CO_2 from N_2. Desorption conditions studied for Zeolite 13X were not able to remove all the CO_2 fixed by the zeolite. Thus, Zeolite 13X showed a fast reduction in the capacity of adsorption. Therefore, the feasibility of the Zeolite 13X for DAC in the studied conditions was discarded. On the other hand, Zeolite 4Å showed a higher stability than Zeolite 13X, and a good adsorbent capacity for a physisorbent. Therefore, Zeolite 4Å was considered as an interesting adsorbent for the DAC in the studied conditions. Additionally, adsorption at low temperatures improves the adsorption capacity for Zeolite13X and Zeolite 4Å. The high hydrophilic behaviour found for both zeolites can be an interesting field of study for new adsorbents in water DAC.

7 REFERENCES

Armstrong, Mitchell R., Bohan Shan, Zhenfei Cheng, Dingke Wang, Jichang Liu, and Bin Mu. 2017. “Adsorption and Diffusion of Carbon Dioxide on the Metal-Organic Framework CuBTB.” *Chemical Engineering Science* 167: 10–17. https://doi.org/10.1016/j.ces.2017.03.049.

Basu, Prabir, and Prabir Basu. 2018. “Analytical Techniques.” *Biomass Gasification, Pyrolysis and Torrefaction*, January, 479–95. https://doi.org/10.1016/B978-0-12-812992-0.00023-6.

Bavec, M., M. Robačer, D. Stajnko, T. Vukmanić, and F. Bavec. 2017. *Sustainability of Vegetable Production Systems Evaluated by Ecological Footprint*. *Good Agricultural Practices for Greenhouse Vegetable Production in the South East European Countries. Principles for Susteibnable Intensification of Smallholder Farms*.

Ben-Mansour, R., M. Basha, and N. A.A. Qasem. 2017. “Multicomponent and Multi-Dimensional Modeling and Simulation of Adsorption-Based Carbon Dioxide Separation.” *Computers and Chemical Engineering* 99: 255–70. https://doi.org/10.1016/j.compchemeng.2017.01.040.

Ben-Mansour, R., M. A. Habib, O. E. Bamidele, M. Basha, N. A.A. Qasem, A. Peedikakkal, T. Laoui, and M. Ali. 2016. “Carbon Capture by Physical Adsorption: Materials, Experimental Investigations and Numerical Modeling and Simulations - A Review.” *Applied Energy* 161: 225–55. https://doi.org/10.1016/j.apenergy.2015.10.011.

Bos, M.J., T. Kreuger, S.R.A. Kersten, and D.W.F. Brilman. 2018. “Study on Transport Phenomena and Intrinsic Kinetics for CO2 Adsorption in Solid Amine Sorbent.” *Chemical Engineering Journal*, November. https://doi.org/10.1016/J.CEJ.2018.11.072.

Buijs, Wim, and Stijn De Flart. 2017. “Direct Air Capture of CO2 with an Amine Resin: A Molecular Modeling Study of the CO2 Capturing Process.” *Industrial and Engineering Chemistry Research* 56 (43): 12297–304. https://doi.org/10.1021/acs.iecr.7b02613.

C.D. Keeling, and T.P. Whorf. 2001. *Atmospheric CO2 Records from Sites in the SIO Air*

Sampling Network. Carbon Dioxide Information Analysis Center, Oak Ridge National Laboratory, U.S. Dept. Energy.

Choong, T. S Y, and D. M. Scott. 1998. "The Linear Driving Force Model for Cyclic Adsorption and Desorption: The Effect of External Fluid-Film Mass Transfer." *Chemical Engineering Science* 53 (4): 847–51. https://doi.org/10.1016/S0009-2509(97)00345-X.

Darunte, Lalit A, Krista S Walton, David S Sholl, and Christopher W Jones. 2016. "CO2 Capture via Adsorption in Amine-Functionalized Sorbents." *Current Opinion in Chemical Engineering* 12 (May): 82–90. https://doi.org/10.1016/J.COCHE.2016.03.002.

Do, Duong D. 1998. *Adsorption Analysis: Equilibria and Kinetics*. Vol. 2. https://doi.org/10.1142/p111.

Elfving, Jere. 2015. "CHARACTERIZATION OF AMINE-BASED CO 2 ADSORBENT FOR DIRECT AIR CAPTURE." Lappeenranta University of Technology.

Elfving, Jere, Cyril Bajamundi, and Juho Kauppinen. 2017. "Characterization and Performance of Direct Air Capture Sorbent." *Energy Procedia* 114 (July): 6087–6101. https://doi.org/10.1016/J.EGYPRO.2017.03.1746.

Elfving, Jere, Cyril Bajamundi, Juho Kauppinen, and Tuomo Sainio. 2017. "Modelling of Equilibrium Working Capacity of PSA , TSA and TVSA Processes for CO 2 Adsorption under Direct Air Capture Conditions." *Journal of CO2 Utilization* 22 (April): 270–77. https://doi.org/10.1016/j.jcou.2017.10.010.

European Commission. 2014. "2030 Climate & Energy Framework." *Report*, no. 1: 1–5. https://doi.org/10.1007/s13398-014-0173-7.2.

Farooq, Shamsuzzaman, and Douglas M. Ruthven. 1990. "Heat Effects in Adsorption Column Dynamics. 2. Experimental Validation of the One-Dimensional Model." *Industrial and Engineering Chemistry Research* 29 (6): 1084–90. https://doi.org/10.1021/ie00102a020.

Fasihi, Mahdi, E Olga, and Christian Breyer. 2019. “Techno-Economic Assessment of CO 2 Direct Air Capture Plants” 224. https://doi.org/10.1016/j.jclepro.2019.03.086.

Garshasbi, Vahid, Mansour Jahangiri, and Mansoor Anbia. 2017. “Equilibrium CO 2 Adsorption on Zeolite 13X Prepared from Natural Clays.” *Applied Surface Science* 393: 225–33. https://doi.org/10.1016/j.apsusc.2016.09.161.

Jin, Chongwei, Shaoting Du, Yue Wang, Jason Condon, Xianyong Lin, and Yongsong Zhang. 2009. “Carbon Dioxide Enrichment by Composting in Greenhouses and Its Effect on Vegetable Production.” *Journal of Plant Nutrition and Soil Science* 172: 418–24. https://doi.org/10.1002/jpln.200700220.

Jung, Wonho, Junhyung Park, and Kwang Soon Lee. 2018. “Kinetic Modeling of CO2 Adsorption on an Amine-Functionalized Solid Sorbent.” *Chemical Engineering Science* 177 (February): 122–31. https://doi.org/10.1016/j.ces.2017.11.003.

Kaiser, Harry Mason, and 1956- Drennen Thomas E. 1993. *Agricultural Dimensions of Global Climate Change*. Delray Beach, Fla. : St. Lucie Press. https://www.lib.berkeley.edu/nrlf-electronic-copy/b14921916.

Kimball, B.A., and S.B. Idso. 1983. “Increasing Atmospheric CO2: Effects on Crop Yield, Water Use and Climate.” *Agricultural Water Management* 7 (1–3): 55–72. https://doi.org/10.1016/0378-3774(83)90075-6.

Konduru, Naveen, Peter Lindner, and Nada Marie Assaf-anid. 2015. “Pyrolysis of Heavy Oil in the Presence of Supercritical Water: The Reaction Kinetics in Different Phases.” *AICHE Journal* 61 (3): 857–66. https://doi.org/10.1002/aic.

Kunii, D., and O. Levenspiel. 1991. *Fluidization Engineering*. Edited by Howard Brenner. Elsevier. https://doi.org/10.1016/C2009-0-24190-0.

Marchi, B., S. Zanoni, and M. Pasetti. 2018. “Industrial Symbiosis for Greener Horticulture Practices: The CO2 Enrichment from Energy Intensive Industrial Processes.” *Procedia CIRP* 69 (January): 562–67. https://doi.org/10.1016/J.PROCIR.2017.11.117.

Morin, Mathieu, Sébastien Pécate, Enrica Masi, and Mehrdji Hémati. 2017. “Kinetic Study

and Modelling of Char Combustion in TGA in Isothermal Conditions." *Fuel* 203: 522–36. https://doi.org/10.1016/j.fuel.2017.04.134.

Muñoz, P., A. Antón, M. Nuñez, A. Paranjpe, J. Ariño, X. Castells, J. I. Montera, and J. Rieradevall. 2008. "Comparing the Environmental Impacts of Greenhouse versus Open-Field Tomato Production in the Mediterranean Region." *Acta Horticulturae* 801 PART 2 (February 2019): 1591–96. https://doi.org/10.17660/ActaHortic.2008.801.197.

Nagy, Endre, and Endre Nagy. 2019. "Membrane Gas Separation." *Basic Equations of Mass Transport Through a Membrane Layer*, January, 457–81. https://doi.org/10.1016/B978-0-12-813722-2.00018-2.

Nations, United. 2019. "No Title." United Natios . Department of Economic and Social Affairs. 2019. https://www.un.org/development/desa/publications/world-population-prospects-2019-highlights.html.

Parajuli, Ranjan, Greg Thoma, and Marty D. Matlock. 2019. "Environmental Sustainability of Fruit and Vegetable Production Supply Chains in the Face of Climate Change: A Review." *Science of the Total Environment* 650: 2863–79. https://doi.org/10.1016/j.scitotenv.2018.10.019.

Park, Yongha, Youngsan Ju, Dooyong Park, and Chang Ha Lee. 2016. "Adsorption Equilibria and Kinetics of Six Pure Gases on Pelletized Zeolite 13X up to 1.0 MPa: CO2, CO, N2, CH4, Ar and H2." *Chemical Engineering Journal* 292: 348–65. https://doi.org/10.1016/j.cej.2016.02.046.

Pérez, J A, and C T Ariso. 2008. *Problemas de Transferencia de Materia*. Textos Docentes. Prensas Universitarias de Zaragoza. https://books.google.fi/books?id=4OkpQwAACAAJ.

Perry, S, Robert H Perry, Don W Green, and James O Maloney. 1999. *Chemical Engineers ' Handbook Seventh*.

Pessarakli, Mohammad. 2005. "Handbook of Photosynthesis, Second Edition." *Reactions*.

https://doi.org/10.1201/9781420027877.

Poudel, Megha, and Bruce Dunn. 2017. “Greenhouse Carbon Dioxide Supplementation.” *Oklahoma Cooperative Extension Service* HLA6723 (March): 1–6. http://osufacts.okstate.edu.

Prior, S A, H A Torbert, G B Runion, and H H Rogers. 2003. “Implications of Elevated CO2-Induced Changes in Agroecosystem Productivity.” *Journal of Crop Production* 8 (1–2): 217–44. https://doi.org/10.1300/J144v08n01_09.

Prior, Stephen, Stephen A Prior, G Brett Runion, S Christopher Marble, Hugo H Rogers, and Charles H Gilliam. 2011. “A Review of Elevated Atmospheric CO2 Effects on Plant Growth and Water Relations: Implications for Horticulture.” *HortScience* 46 (2): 158–62.

Ruthven, Douglas M. 1984. *Principles of Adsorption and Adsorption Processes*.

———. 2000. “Rectangular Isotherm Model for Adsorption Kinetics.” *Adsorption* 6 (4): 287–91. https://doi.org/10.1023/A:1026504730443.

Sanz-Pérez, Eloy S., Christopher R. Murdock, Stephanie A. Didas, and Christopher W. Jones. 2016. “Direct Capture of CO2from Ambient Air.” *Chemical Reviews* 116 (19): 11840–76. https://doi.org/10.1021/acs.chemrev.6b00173.

Sarker, Ariful Islam, Adisorn Aroonwilas, and Amornvadee Veawab. 2017. “Equilibrium and Kinetic Behaviour of CO2 Adsorption onto Zeolites, Carbon Molecular Sieve and Activated Carbons.” *Energy Procedia* 114 (November 2016): 2450–59. https://doi.org/10.1016/j.egypro.2017.03.1394.

Serna-Guerrero, Rodrigo, and Abdelhamid Sayari. 2010. “Modeling Adsorption of CO2 on Amine-Functionalized Mesoporous Silica. 2: Kinetics and Breakthrough Curves.” *Chemical Engineering Journal* 161 (1–2): 182–90. https://doi.org/10.1016/jcej.2010.04.042.

Sha, W., X. Wu, K.G. Keong, W. Sha, X. Wu, and K.G. Keong. 2011. “Modelling the Thermodynamics and Kinetics of Crystallisation of Nickel–Phosphorus (Ni–P)

Deposits." *Electroless Copper and Nickel–Phosphorus Plating*, January, 183–217. https://doi.org/10.1533/9780857090966.2.183.

Shafeeyan, Mohammad Saleh, Wan Mohd Ashri Wan Daud, and Ahmad Shamiri. 2014. "A Review of Mathematical Modeling of Fixed-Bed Columns for Carbon Dioxide Adsorption." *Chemical Engineering Research and Design* 92 (5): 961–88. https://doi.org/10.1016/j.cherd.2013.08.018.

Siriwardane, R. V., M. S. Shen, E. P. Fisher, and J. A. Poston. 2001. "Adsorption of CO2 on Molecular Sieves and Activated Carbon." *Energy and Fuels* 15 (2): 279–84. https://doi.org/10.1021/ef000241s.

Valkovska, Dimitrina S., and Krassimir D. Danov. 2000. "Determination of Bulk and Surface Diffusion Coefficients from Experimental Data for Thin Liquid Film Drainage." *Journal of Colloid and Interface Science* 223 (2): 314–16. https://doi.org/10.1006/jcis.1999.6657.

Veneman, R., T. Hilbers, D. W.F. Brilman, and S. R.A. Kersten. 2016. "CO2 Capture in a Continuous Gas-Solid Trickle Flow Reactor." *Chemical Engineering Journal* 289: 191–202. https://doi.org/10.1016/j.cej.2015.12.066.

Veneman, Rens, Natalia Frigka, Wenying Zhao, Zhenshan Li, Sascha Kersten, and Wim Brilman. 2015. "Adsorption of H2O and CO2 on Supported Amine Sorbents." *International Journal of Greenhouse Gas Control* 41 (October): 268–75. https://doi.org/10.1016/J.IJGGC.2015.07.014.

Wang, Tao, Jie Huang, Xin He, Jiayang Wu, Mengxiang Fang, and Jun Cheng. 2014. "CO2 Fertilization System Integrated with a Low-Cost Direct Air Capture Technology." *Energy Procedia* 63 (January): 6842–51. https://doi.org/10.1016/J.EGYPRO.2014.11.718.

Wang, Tao, Jun Liu, Hao Huang, Mengxiang Fang, and Zhongyang Luo. 2016. "Preparation and Kinetics of a Heterogeneous Sorbent for CO2 Capture from the Atmosphere." *Chemical Engineering Journal* 284 (January): 679–86. https://doi.org/10.1016/j.cej.2015.09.009.

Wang, Xia, Linlin Chen, and Qingjie Guo. 2015. “Development of Hybrid Amine-Functionalized MCM-41 Sorbents for CO2capture.” *Chemical Engineering Journal* 260: 573–81. https://doi.org/10.1016/j.cej.2014.08.107.

Wheeler, T.A., M.G. Anderson, S.A. Russell, J.E. Woodward, and B.G. Mullinix. 2015. “Application Pressure and Carrier Volume Affects the Concentration of Azoxystrobin on Peanut Foliage and in Soil.” *Peanut Science* 42 (2): 128–37. https://doi.org/10.3146/0095-3679-42.2.128.

Yang, J., and C.-H. Lee. 1998. “Adsorption Dynamics of a Layered Bed PSA for H<inf>2</Inf> Recovery from Coke Oven Gas.” *AIChE Journal* 44 (6): 1325–34. https://doi.org/10.1002/aic.690440610.

Yang, Yun, and Shimin Liu. 2019. “Estimation and Modeling of Pressure-Dependent Gas Diffusion Coefficient for Coal: A Fractal Theory-Based Approach.” *Fuel* 253 (October): 588–606. https://doi.org/10.1016/j.fuel.2019.05.009.

Zamora, Francisco, Eduardo Sabio, Silvia Román, Carmen María González-García, and Beatriz Ledesma. 2010. “Modelling the Adsorption of P-Nitrophenol by the Boyd Method in Conjunction with the Finite Element Method.” *Adsorption Science and Technology* 28 (8–9): 671–87. https://doi.org/10.1260/0263-6174.28.8-9.671.

Zarghampoor, M. H., M. Mozaffarian, M. Soleimani, and M. Takht Ravanchi. 2017. “Modeling of CO2 Adsorption on Activated Carbon and 13X Zeolite via Vacuum Swing Adsorption.” *IOP Conference Series: Materials Science and Engineering* 206 (1). https://doi.org/10.1088/1757-899X/206/1/012004.

Appendix I

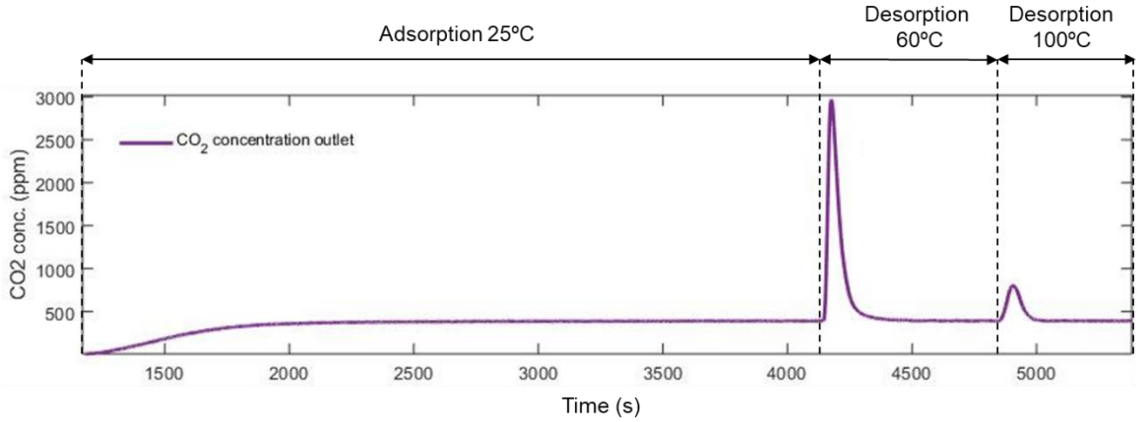

Appendix Figure 1. TSA adsorption-desorption cycle for amine-resin sample. Two desorption steps 60ºC and 100ºC.

In the figure is presented the three steps carried out for the adsorption-desorption cycle for a amine-resin sample. The sample was regenerated with a flow of 1L/min of pure N_2 at 100ºC. The adsorption step showed the typical behaviour of an adsorption with the break curve. The adsorption step was considered ended when the CO_2 concentration in the Fixed-Bed outlet showed a constant value of 400 ppm. Desorption at 60ºC showed a pic of 3000 ppm of concentration. The shortest pic at 100ºC showed that most of the CO_2 fixed by the amine was removed at 60ºC. LabVIEW was used to calculate the capacity of adsorption and desorption. The adsorption capacity was calculated as the integral of the area over the curve until 400 ppm. For the desorption capacity the program integrated the area under the pic until 400 ppm.

Appendix II

At Appendix Figure 2 is observed a Zoom of the adsorption capacity results from the Zeolite 4Å. It is observed that linear behaviour for the zeolite ended for times <60 seconds.

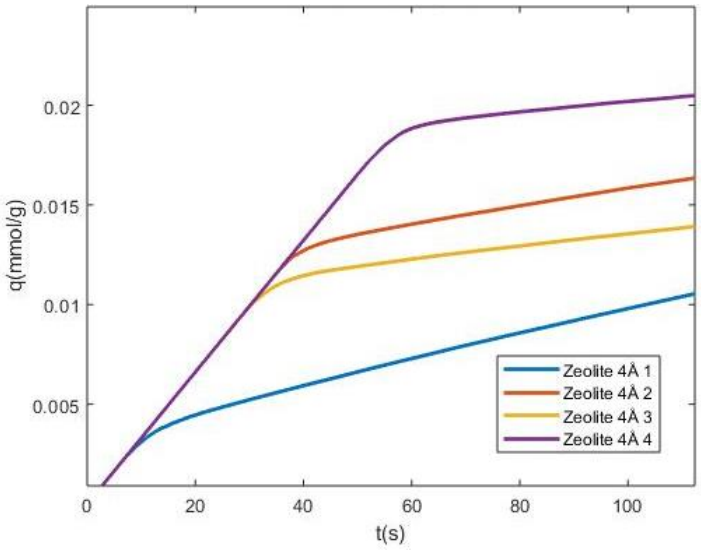

Appendix Figure 2. Zoom of the adsorption capacity of Zeolite 4Å from fixed-bed.

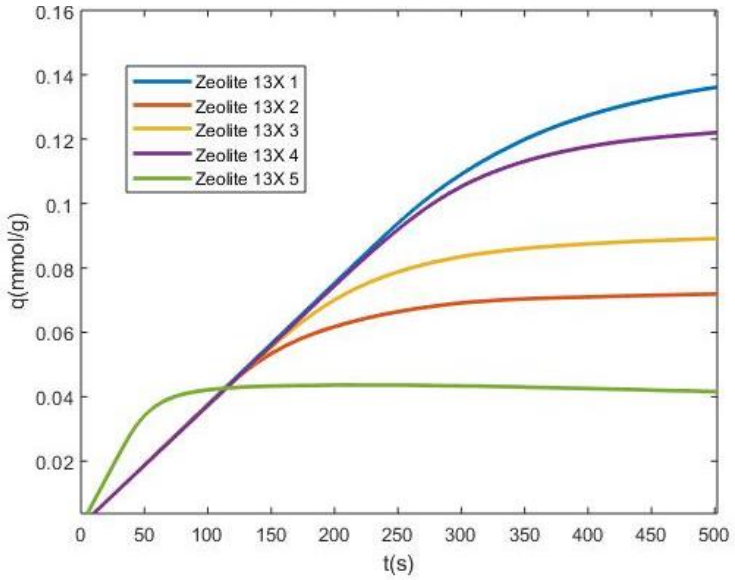

Appendix Figure 3. Zoom of the adsorption capacity of Zeolite 13X from fixed-bed.

Appendix III

Appendix Table 1. Amine-resin experiment conditions and properties for the diffusion coefficient calculation. Fixed-bed.

Amine-resin fixed-bed		
Temperature(K)	T	2.9815E+02
Density of fluid (kg/m^3)	ρf	1.2434E+00
Bed Voidage	Ɛ	5.3970E-01
Length column (m)	Lc	4.7000E-02
Diameter Column (m)	D_{colum}	9.0000E-03
Radio thermopar (m)	rth	1.0000E-03
Length of thermopar (m)	L_1	3.7000E-02
Length of column without thermopar (m)	L_2	1.0000E-02
Volume column (m^3)	Vc	2.9900E-06
Volume thermopar (m^3)	Vt	1.1624E-07
V column useful (m^3)	Vc-Vt	2.8738E-06
Area thermopar (m^2)	A_{thermo}	3.1416E-06
Area column (m^2)	A_{column}	6.3617E-05
Area donut ($A_{thermo} - A_{column}$) (m^2)	A_{donut}	6.0476E-05
Volume donut (m3)	V_{donut}	1.2095E-06
m solid needed (kg)	m_s	5.4293E-04
Particle porosity ($V_{void\ particle}/V_{total\ particle}$)	Ɛp	3.1000E-01
Viscosity fluid (Pa·s)	μ	1.7716E-05
Radio particle (m)	R_p	3.0000E-04
Radio pore (m)	r_p	7.2550E-09
skeletal density (kg/m^3)	ρs	1.0246E+00
particle density (kg/m^3)	ρp	7.0697E+02
bulk density (kg/m^3)	ρb	4.4889E+02
Cross-sectional area(m^2)	A	6.3617E-05
Superficial velocity ($\dot{V}/A_{column}$) (m/s)	v	2.6198E-01
Interstitial velocity (m/s)	vi	4.8542E-01
Volumetric flow (m^3/s)	$\dot{V}$	1.6667E-05
Volumetric flow (L/ min)	$\dot{V}$	1.0000E+00
Reynolds of particle	Re	1.1033E+01
Molecular diffusion coefficient (m^2/s)	$D_{CO2/N2}$	1.42588E-05
Schmidt Number	Sc	9.9923E-01
Sherwood Number	Sh	5.1982E+00
External diffusion coefficient (m/s)	kg	1.2353E-01
Knudsen diffusion coefficient CO_2 (m^2/s)	D_{KCO_2}	1.8317E-06
Knudsen diffusion coefficient N_2 (m^2/s)	D_{KN_2}	2.2959E-06
Tortuosity	-	2.1000E+00

Effective Knudsen diffusion coefficient CO_2 (m^2/s)	$D_{Keff,\ CO_2}$	2.7039E-07
Effective Knudsen diffusion coefficient N_2 (m^2/s)	$D_{Keff,\ N_2}$	3.3891E-07
Effective molecular diffusion coefficient CO2/N2 (m^2/s)	$D_{meff\ CO_2/N_2}$	2.1049E-06
Free path (m)	λ	4.1232E-08
Nudsen number	N_K or K_n	2.8416E+00
Equivalent diffusivity Poiseuille (m^2/s)	D_v	4.0853E-08
Effective diffusivity Poiseuille (m^2/s)	D_{veff}	1.4942E-05
Axial Dispersion coefficient (m^2/s)	D_z	6.7402E-04

Appendix Table 2. Amine-resin experiment conditions and properties for the diffusion coefficient calculation. TGA.

Amine-resin TGA		
Temperature(K)	T	2.9815E+02
Density of fluid (kg/m^3)	ρf	1.2434E+00
Mass of solid needed (kg)	m_s	5.4293E-04
Particle porosity ($V_{void\ particle}/V_{total\ particle}$)	Ɛp	3.1000E-01
Viscosity fluid (Pa·s)	μ	1.7716E-05
Radio particle (m)	rparticle	3.0000E-04
Radio pore (m)	rpore	7.2550E-09
Skeletal density (kg/m^3)	ρs	1.0246E+00
Particle density (kg/m^3)	ρp	7.0697E+02
Bulk density (kg/m^3)	ρb	4.4889E+02
Cross-sectional area(m^2)	S	1.25664E-05
Superficial velocity ($\dot{V}/A_{column}$) (m/s)	v	6.6315E-02
Volumetric flow (m^3/s)	$\dot{V}$	8.3333E-07
Volumetric flow (L/ min)	$\dot{V}$	5.0000E-02
Reynolds of particle	Re	2.7926E+00
Molecular diffusion coefficient (m^2/s)	D_{CO_2/N_2}	1.4259E-05
Schmidt Number	Sc	9.9923E-01
Sherwood Number	Sh	2.6153E+00
External diffusion coefficient (m/s)	kg	6.2151E-02
Knudsen diffusion coefficient CO_2 (m^2/s)	D_{KCO_2}	1.8317E-06
Knudsen diffusion coefficient N_2 (m^2/s)	D_{KN_2}	2.2959E-02
Tortuosity	-	2.1000E+00
Effective Knudsen diffusion coefficient CO_2 (m^2/s)	$D_{Keff,\ CO_2}$	2.7039E-07
Effective Knudsen diffusion coefficient N_2 (m^2/s)	$D_{Keff,\ N_2}$	3.3891E-07
Effective molecular diffusion coefficient CO2/N2 (m2/s)	$D_{meff\ CO_2/N_2}$	2.1049E-06
Free path (m)	λ	4.1232E-08
Knudsen number	N_K or K_n	2.8416E+00
Equivalent diffusivity Poiseuille (m^2/s)	D_v(m2/s)	4.0853E-08
Effective diffusivity Poiseuille (m^2/s)	D_{veff}(m2/s)	1.4942E-05

Appendix Table 3. Zeolite 13X experiment conditions and properties for the diffusion coefficient calculation. Fixed-bed.

Zeolite 13X Fixed-bed		
Temperature(K)	T	2.9815E+02
Density of fluid (kg/m^3)	ρf	1.2434E+00
Bed Voidage	Ɛ	4.7154E-01
Length column (m)	Lc	4.7000E-02
Diameter Column (m)	D_{colum}	9.0000E-03
Radio thermopar (m)	rth	1.0000E-03
Length of thermopar (m)	L_1	3.7000E-02
Length of column without thermopar (m)	L_2	1.0000E-02
Volume column (m^3)	Vc	2.9900E-06
Volume thermopar (m^3)	Vt	1.1624E-07
V column useful (m^3)	Vc-Vt	2.8738E-06
Area thermopar (m^2)	A_{thermo}	3.1416E-06
Area column (m^2)	A_{column}	6.3617E-05
Area donut ($A_{thermo} - A_{column}$) (m^2)	A_{donut}	6.0476E-05
Volume donut (m^3)	V_{donut}	1.2095E-06
m solid needed (kg)	m_s	7.8618E-04
Particle porosity ($V_{void\ particle}/V_{total\ particle}$)	Ɛp	3.7000E-01
Viscosity fluid (Pa·s)	μ	1.7716E-05
Radio particle (m)	R_p	2.1350E-04
Radio pore (m)	r_p	6.5000E-10
skeletal density (kg/m^3)	ρs	1.9524E+03
particle density (kg/m^3)	ρp	1.2300E+03
bulk density (kg/m^3)	ρb	6.5000E+02
Cross-sectional area(m^2)	S	6.3617E-05
Superficial velocity ($\dot{V}/A_{column}$) (m/s)	v	2.6198E-01
Interstitial velocity (m/s)	vi	5.5559E-01
Volumetric flow (m^3/s)	$\dot{V}$	1.6667E-05
Volumetric flow (L/ min)	$\dot{V}$	1.0000E+00
Reynolds of particle	Re	7.8515E+00
Molecular diffusion coefficient (m^2/s)	$D_{CO2/N2}$	1.42588E-05
Schmidt Number	Sc	9.9833E-01
Sherwood Number	Sh	4.6900E+00
External diffusion coefficient (m/s)	kg	1.5675E-01
Knudsen diffusion coefficient CO_2 (m^2/s)	D_{KCO2}	1.6411E-07
Knudsen diffusion coefficient N_2 (m^2/s)	D_{KN2}	2.0569E-03
Tortuosity	-	2.1000E+00
Effective Knudsen diffusion coefficient CO_2 (m^2/s)	$D_{Keff,\ CO2}$	2.8914E-08
Effective Knudsen diffusion coefficient N_2 (m^2/s)	$D_{Keff,\ N2}$	3.6241E-08
Effective molecular diffusion coefficient CO2/N2 (m^2/s)	$D_{meff\ CO2/N2}$	2.5145E-06

Free path (m)	λ	4.1232E-08
Nudsen number	N_K or K_n	3.1717E+01
Equivalent diffusivity Poiseuille (m^2/s)	D_v	3.2792E-10
Effective diffusivity Poiseuille (m^2/s)	D_{veff}	1.4315E-07
Axial Dispersion coefficient (m^2/s)	D_z	7.2393E-04

Appendix Table 4. Zeolite 4Å experiment conditions and properties for the diffusion coefficient calculation. Fixed-bed.

Zeolite 4Å fixed-bed			
Properties/Conditions		Pellet	Powder
Temperature(K)	T	2.9815E+02	2.9815E+02
Density of fluid (kg/m^3)	ρf	1.2434E+00	1.2434E+00
Bed Voidage	Ɛ	1.7558E-01	2.8267E-05
Length column (m)	Lc	4.7000E-02	4.7000E-02
Diameter Column (m)	D_{colum}	9.0000E-03	9.0000E-03
Radio thermopar (m)	rth	1.0000E-03	1.0000E-03
Length of thermopar (m)	L_1	3.7000E-02	3.7000E-02
Length of column without thermopar (m)	L_2	1.0000E-02	1.0000E-02
Volume column (m^3)	Vc	2.9900E-06	2.9900E-06
Volume thermopar (m^3)	Vt	1.1624E-07	1.1624E-07
V column useful (m^3)	Vc-Vt	2.8738E-06	2.8738E-06
Area thermopar (m^2)	A_{thermo}	3.1416E-06	3.1416E-06
Area column (m^2)	A_{column}	6.3617E-05	6.3617E-05
Area donut ($A_{thermo} - A_{column}$) (m^2)	A_{donut}	6.0476E-05	6.0476E-05
Volume donut (m3)	V_{donut}	1.2095E-06	1.2095E-06
m solid needed (kg)	m_s	8.8585E-04	4.4776E-04
Particle porosity ($V_{void\ particle}/V_{total\ particle}$)	Ɛp	2.1500E-01	3.1455E-01
Viscosity fluid (Pa·s)	μ	1.7716E-05	1.7716E-05
Radio particle (m)	R_p	2.0300E-03	4.4000E-05
Radio pore (m)	r_p	2.0000E-10	2.0000E-10
skeletal density (kg/m^3)	ρs	1.1317E+03	5.4010E+02
particle density (kg/m^3)	ρp	8.8838E+02	3.7021E+02
bulk density (kg/m^3)	ρb	7.3240E+02	3.7020E+02
Cross-sectional area(m^2)	S	6.3617E-05	6.3617E-05
Superficial velocity ($\dot{V}/A_{column}$) (m/s)	v	2.6198E-01	2.6198E-01
Interstitial velocity (m/s)	vi	1.4921E+00	9.2681E+03
Volumetric flow (m^3/s)	$\dot{V}$	1.6667E-05	1.6667E-05
Volumetric flow (L/ min)	$\dot{V}$	1.0000E+00	1.0000E+00
Reynolds of particle	Re	7.4654E+01	1.6181E+00
Molecular diffusion coefficient (m^2/s)	$D_{CO2/N2}$	1.4272E-05	1.4272E-05
Schmidt Number	Sc	9.9833E-01	9.9833E-01

Sherwood Number	Sh	2.3700E+01	2.7499E+02
External diffusion coefficient (m/s)	kg	8.3309E-02	4.4598E+01
Knudsen diffusion coefficient CO_2 (m^2/s)	D_{KCO2}	2.3700E+01	5.0494E-04
Knudsen diffusion coefficient N_2 (m^2/s)	D_{KN2}	8.3309E-02	6.3291E-08
Tortuosity	-	1.6000E-02	2.0380E+00
Effective Knudsen diffusion coefficient CO_2 (m^2/s)	$D_{Keff,\ CO2}$	6.7852E-07	7.7935E-09
Effective Knudsen diffusion coefficient N_2 (m^2/s)	$D_{Keff,\ N2}$	8.5047E-07	9.7685E-09
Effective molecular diffusion coefficient CO2/N2 (m^2/s)	$D_{meff\ CO2/N2}$	1.9178E-04	2.2027E-06
Free path (m)	λ	4.1232E-08	4.1232E-08
Nudsen number	N_K or K_n	1.0308E+02	1.0308E+02
Equivalent diffusivity Poiseuille (m^2/s)	D_v	3.1046E-11	3.1046E-07
Effective diffusivity Poiseuille (m^2/s)	D_{veff}	1.0336E-06	3.1046E-11
Axial Dispersion coefficient (m^2/s)	D_z	4.6546E-03	1.1872E-08

Appendix Table 5. Coefficients for the calculation of the molecular diffusion.

Coefficients for Chapman-Enskog	
T (K)	2.9800E+02
P (Pa)	1.1000E+05
P (atm)	1.0856E+00
P(dynas/cm2)	1.1000E+04
σ_{CO2}(Å)	3.9410E+00
σ_{N2}(Å)	3.7980E+00
ε_{CO2}/kb (K)	1.9520E+02
ε_{N2}/kb (K)	7.1400E+01
$\sigma_{CO2,N2}$(Å)	3.8695E+00
$\varepsilon_{CO2,N2}$/kb (K)	1.1806E+02
$T \cdot kb/\varepsilon_{CO2,N2}$	2.5242E+00
Ω_D	9.9674E-01
$M_{CO2,N2}$ $(g/mol)^{-1}$	5.8420E-02
$D_{mCO2/N2}$ (cm2/s)	1.4259E-01
$D_{mCO2/N2}$ (m2/s)	1.4259E-05

The previous table only has dependence from the gas mixture composition and the temperature and pressure experimental conditions. Thus, this table can be used for all the experiments carried out.

The gas viscosity for the pure components was calculated following the relation recommended by Perry et al. (1999). The correlation took in consideration the dependence of the viscosity to the temperature, assuming negligible the pressure contribution in comparison with the temperature. The method is able to predict accurate results for low pressures as the experimental conditions (Perry et al. 1999).

$$\mu = \frac{C1T^{C2}}{1 + C3/T + C4/T^2}$$

Where:

- μ: Viscosity (Pa·s).
- Ci: Characteristic coefficient for the gas (dimensionless).
- T: Temperature (K)

As the adsorption experiments were carried out using a binary mix of pure gases, the viscosity of the mixture was calculated from the correlation of Wilke for binary mixtures.

$$\mu = \frac{y_1\mu_1}{y_1 + y_2\phi_{12}} + \frac{y_2\mu_2}{y_2 + y_1\phi_{21}}$$

Where:

- y_1: Molar fraction of gas 1.
- y_1: Molar fraction of gas 1.
- μ_1: Viscosity gas 1.
- μ_2: Viscosity gas 2.
- ϕ_{12}: Dimensionless number.

The coefficients ϕ_{12} and ϕ_{21} were calculated as :

$$\phi_{ij} = \frac{1}{\sqrt{8}}\left(1 + \frac{M_i}{M_j}\right)^{-1/2}\left(1 + \left(\frac{\mu_i}{\mu_j}\right)^{1/2}\left(\frac{M_j}{M_i}\right)^{1/4}\right)^2 ; \phi_{ji} = \frac{\mu_j}{\mu_i}\frac{M_i}{M_j}\,\phi_{ij}$$

Where:

- M_i : Molecular weight of the compound i. (Kg/mol)
- M_j: Molecular weight of the compound j. (Kg/mol)

The coefficients for the Wilke correlations and the viscosity results are presented at **Appendix Table 6** and **Appendix Table 7**. In addition, air viscosity at the experimental conditions was calculated and it is presented at tabe X in order to be able to use it for the future experiments.

Appendix Table 6. Coefficients for N_2 and CO_2 viscosity.

Calculation μ N_2		Calculation μ CO_2	
Temperature (K)	2.9815E+02	Temperature (K)	2.9815E+02
P (Pa)	1.1000E+05	P (Pa)	1.1000E+05
C1	6.5592E-07	C1	2.1480E-06
C2	6.0810E-01	C2	4.6000E-01
C3	5.4714E+01	C3	2.9000E+02
C4	0.0000E+00	C4	0.0000E+00
M (g/mol)	2.8013E+01	M (g/mol)	4.4010E+01
M (kg/mol) SI	2.8013E-02	M (kg/mol) SI	4.4010E-02
μ $_{N2}$ (Pa·s)	1.7717E-05	μ $_{CO2}$ (Pa·s)	1.4970E-05
μ $_{N2}$ (Poise)	1.7717E-06	μ $_{CO2}$ (Poise)	1.4970E-06
ρ $_{N2}$ (kg/m3)	1.2431E+00	ρ $_{CO2}$ (kg/m3)	1.9530E+00

Appendix Table 7. Coefficients for the CO_2/N_2 mixture gas viscosity.

Calculation μ mixture of N_2 + CO_2	
Temperature (K)	2.9815E+02
P (Pa)	1.1000E+05
%CO_2	4.0000E-02
%N_2	9.9960E+01
Y_{CO2}	4.0000E-04
Y_{N2}	9.9960E-01
M	2.8019E+01
M, SI	2.8019E-02
μ mix (ideal gases)	1.7716E-05
μ mix (Poise)	1.7716E-06
ρ mix (ideal gases)	1.2434E+00
ϕ $_{CO2/N2}$	7.3121E-01
ϕ $_{N2/CO2}$	1.3596E+00
μ $_{mix}$ (Wilke)	1.7715E-05

Appendix Table 8. Coefficients for atmospheric air composition.

Calculation μ CO_2	
Temperature(K)	2.9815E+02
P (Pa)	1.1000E+05
C1	1.4250E-06
C2	5.0390E-01
C3	1.0830E+02
C4	0.0000E+00
M (g/mol)	2.8960E+01
M (kg/mol) SI	2.8960E-02
μ_{Air} (Pa·s)	1.8455E-05
μ_{Air} (Poise)	1.8455E-06
ρ_{Air} (kg/m3)	1.2851E+00

From the **Appendix Table 6** and **Appendix Table 7** can be observed that the properties of the mixture presented approximately the same values than for pure N2. In addition, the viscosity found for air differed from the adsorption mixture viscosity. Thus, for air experiments the changes in the viscosity should be taken in account.

ANEXO II: ECUACIONES EMPLEADAS

CINÉTICAS DE CAPTURA DE CO_2 DEL AIRE BASADAS EN ADSORCIÓN

KINETICS OF ADSORPTION-BASED DIRECT AIR CAPTURE

Autor

Víctor Daniel Mercader Plou

Director

Jere Elfving (VTT Finlandia)

Ponente

José Ángel Peña

Máster en Ingeniería Química

ESCUELA DE INGENIERÍA Y ARQUITECTURA

2020

ÍNDICE

ÍNDICE DE TABLAS

LISTADO DE SÍMBOLOS Y ABREVIACIONES

A_{column}	Cross sectional column area / Área transversal de la columna
A_{thermo}	Cross sectional thermopar area / Area transversal del termopar
C	Concentration / Concentración
DAC	Direct Air Capture / Captura de Aire Directa
D	Diffusivity coefficient / Coeficiente de difusión
D_{colum}	Column diameter / Diámetro de la columna
D_{ef}	Effective diffusivity coefficient of the diffusive compound in the pores / Coeficiente de difusión efectivo del componente difusivo en los poros
D_K	Knudsen diffusivity coefficient / Coeficiente de difusión Knudsen
D_{Kef}	Knudsen effective coefficient / Coeficiente efectivo de difusión Knudsen
D_L	Axial dispersion coefficient, also referred as D_z Coeficiente de dispersion Axial, también referenciado como D_z /
D_m	Molecular diffusivity coefficient / Coeficiente de difusión molecular
d_p	Pore diameter / Diámetro de poro
D_p	Particle diameter / Diámetro de partícula
D_{pi}	Pore diffusivity coefficient / Coeficiente de difusión en el poro
D_v	Viscous diffusivity coefficient / Coeficiente de difusión en flujo viscoso
D_{vef}	Effective viscous diffusivity coefficient / Coeficiente efectivo de difusión en flujo viscoso

FAO	Food and Agriculture Organization of the United Nations
J	Molecular flux / Flujo molar
k_f	External mass transfer coefficient, also referred as k_g / Coeficiente externo de transferencia de materia, también descrito como k_g
L_1	Length of thermopar / Longitud del termopar
L_2	Length of column without thermopar / Longitud de la columna (lecho) sin termopar
L_c	Column length / Longitud de la columna de adsorción (lecho de partículas)
M_i	Molecular weight of compound / Peso molecular del compuesto/elemento i
MOF	Metal–organic framework
P	Total pressure / Presión total
P_i	Partial pressure of compound i / Presión parcial del componente i
q	Adsorption capacity / Capacidad de adsorción
q_e	Adsorption equilibrium capacity / Capacidad de adsorción en el equilibrio
T	Temperature / Temperatura
R_c	Radio column / Radio de la columna de adsorción (lecho)
R_g	Ideal gases constant / Constante de los gases ideales
r_p	Pore radius / Radio de poro
R_p	Particle radius / Radio de partícula
S	Cross sectional area / Área transversal

v	Superficial velocity, also referred as u_o /
	Velocidad superficial, también referenciada como u_o
vi	Interstitial velocity / Velocidad intersticial
V_c	Column volume / Volumen de la columna de adsorción (lecho)
Vt	Thermopar volume / Volumen del termopar
V_p	Volume of particle / Volumen de la partícula de adsorbente
v_p	Volume of pore / Volumen de poro
$\dot{V}$	Volumetric flow rate / Caudal volumétrico
Y_i	Molar fraction of the compound i / Fracción molar del componente i

DIMENSIONLESS NUMBERS

Re_p	Reynolds of particle / Número de Reynolds de partícula
S_c	Schmidt number / Número de Schmidt
S_h	Sherwood / Número de Sherwood
K_n	Knudsen number, also referred as N_K /
	Número de Knudsen también referenciado como N_K

GREEK SIMBOLS

ρ_f	Fluid density / Densidad del fluido
ρ_b	Bulk density / Densidad aparente
ρ_s	Skeletal density / Densidad de la fracción de sólido
ρ_p	Particle density / Densidad de partícula

μ	Fluid viscosity / Viscosidad del fluido
λ	Free path / Camino libre medio
Ω_D	Integral collision coefficient / Integral de colisión
σ^2	Characteristic length (Å) / Longitud característica (Å)
ε	Bed porosity, also referred as voidage / Porosidad de lecho, fracción hueca
ε_p	Particle porosity / Porosidad de partícula
τ	Tortuosity factor / Factor de tortuosidad

I. ANEXO II

Tabla 1. Ecuaciones empleadas en los cálculos

Nombre	Ecuación	Nº Ecuación	Referencia
Fick law	$J = -D\frac{\partial c}{\partial x}$	Eq.1	Ruthven (1984) and Do (1998)
Chapman-Enskog	$D_{m12} = \frac{0.001858\, T^{3/2}(1/M_1 + 1/M_2)^{1/2}}{P\sigma_{12}^2\Omega_{D,12}}$	Eq.2	Do (1998)
Molecular diffusivity	$D_p = \frac{D_m}{\tau}$	Eq.3	Ruthven (1984)
Porosity of particle	$\varepsilon_p = \rho_s * V_p\ ;\ \rho_p = (1-\varepsilon_p) * \rho_s$	Eq.4	Ruthven (1984); Pérez and Ariso (2008)
Estimation of pore volume	$\frac{V_p}{S_g} = \frac{\pi {r_p}^2 L_p}{2\pi r_p L_p} = \frac{r_p}{2}$	Eq.5	Ruthven (1984); Pérez and Ariso (2008)
Fick law in terms of Eq.4 and Eq.5	$J = -\varepsilon_p D_p \frac{\partial c}{\partial x}$	Eq.6	Ruthven (1984)
Fick law for effective pore diffusion coefficient	$J = -D_{ef}\frac{\partial c}{\partial x}\ ;\ D_{ef} = \frac{D_m}{\tau}\varepsilon_p$	Eq.7	Ruthven (1984); Pérez and Ariso (2008)
Diffusivity parameter D_K for Knudsen diffusion	$D_K = 9700\, r_p \left(\frac{T}{M}\right)^{1/2}\ (cm^2 s^{-1})$	Eq.8	Ruthven (1984)
Separation factor Knudsen	$\text{Separation factor Knudsen} = \frac{J_i}{J_j} = \sqrt{\frac{M_j}{M_i}}$	Eq.9	Nagy and Nagy (2019)
Knudsen effective diffusion coefficient	$D_{Kef} = \frac{\varepsilon_p D_K}{\tau}$	Eq.10	Ruthven (1984)

Fick law in terms of Knudsen effective diffusion coefficient	$J = -D_{Kef}\frac{\partial c}{\partial x}$	Eq.11	Ruthven (1984) and Do (1998)
Eq.11 expressed in terms of pressure	$J = -D_{Kef}\frac{\partial c}{\partial x} = -\frac{D_{Kef}}{R_g T}\frac{\partial P}{\partial x}$	Eq.12	Ruthven (1984) and Do (1998)
Knudsen number	$K_n = \frac{\lambda}{d_p}$	Eq.13	Ruthven (1984)
Free path	$\lambda = \frac{3.2\,\mu}{P}\sqrt{\frac{R_g T}{2\pi M_1}}$	Eq.14	Perry et al. (1999)
Evans, Watson and Manson and Scoth and Dullien equation for Diffusion coefficient ($K_n \approx 1$)	$\frac{1}{D_{ef}} = \frac{1}{D_{Kef}} + \frac{1}{D_m}\left[1 - \left(1 + \frac{J_2}{J_1}\right)Y_1\right]$	Eq.15	Perry et al. (1999)
Coefficient of diffusion applied DAC and diluted gas	$\frac{1}{D_{ef}} = \frac{1}{D_{Kef}} + \frac{1}{D_m}$	Eq.16	Deduction based on Perry et al. (1999)
Viscous diffusivity coefficient	$D_v = \frac{P{r_p}^2}{8\mu}$	Eq.17	Ruthven (1984)

The Fick law Eq.1 in terms of viscous flux for a medium pore solid	$J_{vis} = -\frac{\varepsilon_p {r_p}^2}{8\mu\tau}\frac{P}{R_g T}\frac{dP}{dZ} = -\frac{\varepsilon_p {r_p}^2}{8\mu\tau} C R_g T = -D_{vef}\frac{dC}{dZ}$	Eq.18	Do (1998)
Henry Law	$C_s = K_H C_g$	Eq.19	Do (1998); Ruthven (1984); Perry et al. (1999)
The Henry constant in terms of temperature	$K_H = K_{H,\infty} exp(-\Delta H/R_g T)$	Eq.20	Do (1998)
Surface diffusion in terms of temperature	$D_s = D_{s\infty} exp(-E_s/R_g T)$	Eq.21	Do (1998)
Fick law for surface diffusion	$J_s = -(1-\varepsilon_p) D_{s\infty} K_\infty exp\left(-\frac{E_s + \Delta H}{R_g T}\right)\frac{dC}{dz}$	Eq.22	Do (1998)
Linear driving force equation (LDF)	$\frac{\partial \bar{q}}{\partial t} = k \cdot a(c - c^*) = \frac{3k_f}{R_p}(c - c^*)$	Eq.23	Ruthven (1984)
Effective mass transfer coefficient from Ranz and Marshall correlation in dimensionless terms $3 < Re_p < 10^4$	$Sh = \frac{2k_f R_p}{D_m} = \frac{0.357}{\varepsilon} {Re_p}^{0.64} {S_c}^{0.33}$	Eq.24	Ruthven (1984)

Sh proposed by Carberry valid for fluids with Re_p >1	$Sh = \frac{2k_f R_p}{D_m} = 1.1\left(\frac{Re_p}{\varepsilon}\right)^{0.5} Sc^{0,33}$	Eq.24*	Perry et al. (1999)
Axial Dispersion correlation suggested by Wakao	$\frac{D_L}{2vR_p} = \frac{20}{\varepsilon}\left(\frac{D_m}{2vR_p}\right) + \frac{1}{2} = \frac{20}{Re_p Sc} + \frac{1}{2}$	Eq.25	Ruthven (1984)
LDF expressed with driving force expressed as a differential of capacity	$\frac{\partial \bar{q}}{\partial t} = k_{LDF}(q - q^*)$	Eq.26	Ruthven (1984) and Perry et al. (1999)
Pseudo-First order model (LDF1)	$\frac{dq}{dt} = k_{LDF1}(q_e - \overline{q})$	Eq.27	Bos et al. (2018).
Pseudo-Second order model (LDF2)	$\frac{dq}{dt} = k_{LDF2}(q_e - \overline{q})^2$	Eq.28	Bos et al. (2018).
Avrami model applied to CO_2 capture modeling	$\frac{dq}{dt} = k_A{}^n t^{n-1}(q_e - \overline{q})$	Eq.29	Jung, Park, and Lee (2018) ; Serna-Guerrero and Sayari (2010)
Veneman model for LDF1 and LDF2 respectively	$\frac{dq}{dt} = k_{V1} p_{CO_2}(q_e - \overline{q})$; $\frac{dq}{dt} = k_{V2}\, p_{CO_2}(q_e - \overline{q})^2$	Eq.30	Rens Veneman et al. (2015 & 2016)
The Farooq and Ruthven LDF constant determination	$\frac{1}{k_i} = \frac{R_p q_0}{3k_f c_0} + \frac{R_p^2 q_0}{15\varepsilon_p D_{pi} c_0} + \frac{r_p^2}{15 D_{\mu i}}$	Eq.31	Shafeeyan e t al. (2014)
The LDF constant included in	$k = \frac{15\Psi(1-\varepsilon)\varepsilon_p D_{pi}}{\Lambda R_p^2}$	Eq.32	Perry et al. (1999)

Perry et al. (1999)			
Ergun equation under minimal fluidization conditions	$\frac{\Delta P_{mf}}{L_{mf}} = 150\frac{(1-\varepsilon_{mf})^2}{{\varepsilon_{mf}}^3}\frac{\mu}{(\Phi D_e)^2}u_m + 1.75\frac{(1-\varepsilon_{mf})}{{\varepsilon_{mf}}^3}\frac{\rho_f}{(\Phi D_e)}{u_m}^2$	Eq.33	Kunii and Levenspiel, Fluidization Engineering (1991)
Eq.33 simplified for $R_{ep} < 20$	$\frac{\Delta P_{mf}}{L_{mf}} = 150\frac{(1-\varepsilon_{mf})^2}{{\varepsilon_{mf}}^3}\frac{\mu}{(\Phi D_e)^2}u_m$	Eq.34	Kunii and Levenspiel, Fluidization Engineering (1991)
Pressure drop under minimal fluidization conditions	$\Delta P_{mf} = \frac{m_s}{S}$	Eq.35	Kunii and Levenspiel, Fluidization Engineering (1991)
Mass transfer balance at fixed-bed model	$-D_L\frac{\partial^2 C}{\partial z^2} + u\frac{\partial C}{\partial z^2} + \frac{\partial C}{\partial t} + \left(\frac{1-\varepsilon}{\varepsilon}\right)\rho_p\frac{\overline{\partial q}}{\partial t} = 0;$	Eq.36	Buijs and De Flart (2017)
Eq.32 modified under conditions explained in section 4.4 of ANEXO I	$\frac{1}{k_i} = \frac{R_p q_0 \rho_B}{3k_f c_0(1-\varepsilon)} + \frac{R_p^2 q_0 \rho_B}{15\varepsilon_p D_p c_0(1-\varepsilon)} + \frac{r_p^2}{15D_p}$	Eq. 1	

1 BIBLIOGRAFÍA

Armstrong, Mitchell R., Bohan Shan, Zhenfei Cheng, Dingke Wang, Jichang Liu, and Bin Mu. 2017. "Adsorption and Diffusion of Carbon Dioxide on the Metal-Organic Framework CuBTB." *Chemical Engineering Science* 167: 10–17. https://doi.org/10.1016/j.ces.2017.03.049.

Basu, Prabir, and Prabir Basu. 2018. "Analytical Techniques." *Biomass Gasification, Pyrolysis and Torrefaction*, January, 479–95. https://doi.org/10.1016/B978-0-12-812992-0.00023-6.

Bavec, M., M. Robačer, D. Stajnko, T. Vukmanić, and F. Bavec. 2017. *Sustainability of Vegetable Production Systems Evaluated by Ecological Footprint*. *Good Agricultural Practices for Greenhouse Vegetable Production in the South East European Countries. Principles for Susteibnable Intensification of Smallholder Farms*.

Ben-Mansour, R., M. Basha, and N. A.A. Qasem. 2017. "Multicomponent and Multi-Dimensional Modeling and Simulation of Adsorption-Based Carbon Dioxide Separation." *Computers and Chemical Engineering* 99: 255–70. https://doi.org/10.1016/j.compchemeng.2017.01.040.

Ben-Mansour, R., M. A. Habib, O. E. Bamidele, M. Basha, N. A.A. Qasem, A. Peedikakkal, T. Laoui, and M. Ali. 2016. "Carbon Capture by Physical Adsorption: Materials, Experimental Investigations and Numerical Modeling and Simulations - A Review." *Applied Energy* 161: 225–55. https://doi.org/10.1016/j.apenergy.2015.10.011.

Bos, M.J., T. Kreuger, S.R.A. Kersten, and D.W.F. Brilman. 2018. "Study on Transport Phenomena and Intrinsic Kinetics for CO_2 Adsorption in Solid Amine Sorbent." *Chemical Engineering Journal*, November. https://doi.org/10.1016/J.CEJ.2018.11.072.

Buijs, Wim, and Stijn De Flart. 2017. "Direct Air Capture of CO_2 with an Amine Resin: A Molecular Modeling Study of the CO_2 Capturing Process." *Industrial and Engineering Chemistry Research* 56 (43): 12297–304. https://doi.org/10.1021/acs.iecr.7b02613.

Do, Duong D. 1998. *Adsorption Analysis: Equilibria and Kinetics*. Vol. 2.

https://doi.org/10.1142/p111.

Elfving, Jere. 2015. “CHARACTERIZATION OF AMINE-BASED CO 2 ADSORBENT FOR DIRECT AIR CAPTURE.” Lappeenranta University of Technology.

Elfving, Jere, Cyril Bajamundi, and Juho Kauppinen. 2017. “Characterization and Performance of Direct Air Capture Sorbent.” *Energy Procedia* 114 (July): 6087–6101. https://doi.org/10.1016/J.EGYPRO.2017.03.1746.

Elfving, Jere, Cyril Bajamundi, Juho Kauppinen, and Tuomo Sainio. 2017. “Modelling of Equilibrium Working Capacity of PSA , TSA and TVSA Processes for CO 2 Adsorption under Direct Air Capture Conditions.” *Journal of CO_2 Utilization* 22 (April): 270–77. https://doi.org/10.1016/j.jcou.2017.10.010.

European Commission. 2014. “2030 Climate & Energy Framework.” *Report*, no. 1: 1–5. https://doi.org/10.1007/s13398-014-0173-7.2.

Farooq, Shamsuzzaman, and Douglas M. Ruthven. 1990. “Heat Effects in Adsorption Column Dynamics. 2. Experimental Validation of the One-Dimensional Model.” *Industrial and Engineering Chemistry Research* 29 (6): 1084–90. https://doi.org/10.1021/ie00102a020.

Fasihi, Mahdi, E Olga, and Christian Breyer. 2019. “Techno-Economic Assessment of CO 2 Direct Air Capture Plants” 224. https://doi.org/10.1016/j.jclepro.2019.03.086.

Garshasbi, Vahid, Mansour Jahangiri, and Mansoor Anbia. 2017. “Equilibrium CO 2 Adsorption on Zeolite 13X Prepared from Natural Clays.” *Applied Surface Science* 393: 225–33. https://doi.org/10.1016/j.apsusc.2016.09.161.

Jin, Chongwei, Shaoting Du, Yue Wang, Jason Condon, Xianyong Lin, and Yongsong Zhang. 2009. “Carbon Dioxide Enrichment by Composting in Greenhouses and Its Effect on Vegetable Production.” *Journal of Plant Nutrition and Soil Science* 172: 418–24. https://doi.org/10.1002/jpln.200700220.

Jung, Wonho, Junhyung Park, and Kwang Soon Lee. 2018. “Kinetic Modeling of CO_2 Adsorption on an Amine-Functionalized Solid Sorbent.” *Chemical Engineering*

Science 177 (February): 122–31. https://doi.org/10.1016/j.ces.2017.11.003.

Kaiser, Harry Mason, and 1956- Drennen Thomas E. 1993. *Agricultural Dimensions of Global Climate Change*. Delray Beach, Fla. : St. Lucie Press. https://www.lib.berkeley.edu/nrlf-electronic-copy/b14921916.

Kimball, B.A., and S.B. Idso. 1983. "Increasing Atmospheric CO_2: Effects on Crop Yield, Water Use and Climate." *Agricultural Water Management* 7 (1–3): 55–72. https://doi.org/10.1016/0378-3774(83)90075-6.

Konduru, Naveen, Peter Lindner, and Nada Marie Assaf-anid. 2015. "Pyrolysis of Heavy Oil in the Presence of Supercritical Water: The Reaction Kinetics in Different Phases." *AICHE Journal* 61 (3): 857–66. https://doi.org/10.1002/aic.

Kunii, D., and O. Levenspiel. 1991. *Fluidization Engineering*. Edited by Howard Brenner. Elsevier. https://doi.org/10.1016/C2009-0-24190-0.

Marchi, B., S. Zanoni, and M. Pasetti. 2018. "Industrial Symbiosis for Greener Horticulture Practices: The CO_2 Enrichment from Energy Intensive Industrial Processes." *Procedia CIRP* 69 (January): 562–67. https://doi.org/10.1016/J.PROCIR.2017.11.117.

Morin, Mathieu, Sébastien Pécate, Enrica Masi, and Mehrdji Hémati. 2017. "Kinetic Study and Modelling of Char Combustion in TGA in Isothermal Conditions." *Fuel* 203: 522–36. https://doi.org/10.1016/j.fuel.2017.04.134.

Muñoz, P., A. Antón, M. Nuñez, A. Paranjpe, J. Ariño, X. Castells, J. I. Montera, and J. Rieradevall. 2008. "Comparing the Environmental Impacts of Greenhouse versus Open-Field Tomato Production in the Mediterranean Region." *Acta Horticulturae* 801 PART 2 (February 2019): 1591–96. https://doi.org/10.17660/ActaHortic.2008.801.197.

Nagy, Endre, and Endre Nagy. 2019. "Membrane Gas Separation." *Basic Equations of Mass Transport Through a Membrane Layer*, January, 457–81. https://doi.org/10.1016/B978-0-12-813722-2.00018-2.

Nations, United. 2019. "No Title." United Natios . Department of Economic and Social

Affairs. 2019. https://www.un.org/development/desa/publications/world-population-prospects-2019-highlights.html.

Parajuli, Ranjan, Greg Thoma, and Marty D. Matlock. 2019. "Environmental Sustainability of Fruit and Vegetable Production Supply Chains in the Face of Climate Change: A Review." *Science of the Total Environment* 650: 2863–79. https://doi.org/10.1016/j.scitotenv.2018.10.019.

Park, Yongha, Youngsan Ju, Dooyong Park, and Chang Ha Lee. 2016. "Adsorption Equilibria and Kinetics of Six Pure Gases on Pelletized Zeolite 13X up to 1.0 MPa: CO_2, CO, N2, CH4, Ar and H2." *Chemical Engineering Journal* 292: 348–65. https://doi.org/10.1016/j.cej.2016.02.046.

Pérez, J A, and C T Ariso. 2008. *Problemas de Transferencia de Materia*. Textos Docentes. Prensas Universitarias de Zaragoza. https://books.google.fi/books?id=4OkpQwAACAAJ.

Perry, S, Robert H Perry, Don W Green, and James O Maloney. 1999. *Chemical Engineers ' Handbook Seventh*.

http://osufacts.okstate.edu.

Ruthven, Douglas M. 1984. *Principles of Adsorption and Adsorption Processes*.

———. 2000. "Rectangular Isotherm Model for Adsorption Kinetics." *Adsorption* 6 (4): 287–91. https://doi.org/10.1023/A:1026504730443.

Sanz-Pérez, Eloy S., Christopher R. Murdock, Stephanie A. Didas, and Christopher W. Jones. 2016. "Direct Capture of $CO_2$from Ambient Air." *Chemical Reviews* 116 (19): 11840–76. https://doi.org/10.1021/acs.chemrev.6b00173.

Sarker, Ariful Islam, Adisorn Aroonwilas, and Amornvadee Veawab. 2017. "Equilibrium and Kinetic Behaviour of CO_2 Adsorption onto Zeolites, Carbon Molecular Sieve and Activated Carbons." *Energy Procedia* 114 (November 2016): 2450–59. https://doi.org/10.1016/j.egypro.2017.03.1394.

Serna-Guerrero, Rodrigo, and Abdelhamid Sayari. 2010. "Modeling Adsorption of CO_2 on Amine-Functionalized Mesoporous Silica. 2: Kinetics and Breakthrough Curves." *Chemical Engineering Journal* 161 (1–2): 182–90. https://doi.org/10.1016/jcej.2010.04.042.

Sha, W., X. Wu, K.G. Keong, W. Sha, X. Wu, and K.G. Keong. 2011. "Modelling the Thermodynamics and Kinetics of Crystallisation of Nickel–Phosphorus (Ni–P) Deposits." *Electroless Copper and Nickel–Phosphorus Plating*, January, 183–217. https://doi.org/10.1533/9780857090966.2.183.

Shafeeyan, Mohammad Saleh, Wan Mohd Ashri Wan Daud, and Ahmad Shamiri. 2014. "A Review of Mathematical Modeling of Fixed-Bed Columns for Carbon Dioxide Adsorption." *Chemical Engineering Research and Design* 92 (5): 961–88. https://doi.org/10.1016/j.cherd.2013.08.018.

Veneman, R., T. Hilbers, D. W.F. Brilman, and S. R.A. Kersten. 2016. "CO_2 Capture in a Continuous Gas-Solid Trickle Flow Reactor." *Chemical Engineering Journal* 289: 191–202. https://doi.org/10.1016/j.cej.2015.12.066.

Veneman, Rens, Natalia Frigka, Wenying Zhao, Zhenshan Li, Sascha Kersten, and Wim Brilman. 2015. "Adsorption of H2O and CO_2 on Supported Amine Sorbents." *International Journal of Greenhouse Gas Control* 41 (October): 268–75. https://doi.org/10.1016/J.IJGGC.2015.07.014.

Wang, Tao, Jie Huang, Xin He, Jiayang Wu, Mengxiang Fang, and Jun Cheng. 2014. "CO_2 Fertilization System Integrated with a Low-Cost Direct Air Capture Technology." *Energy Procedia* 63 (January): 6842–51. https://doi.org/10.1016/J.EGYPRO.2014.11.718.

Wang, Tao, Jun Liu, Hao Huang, Mengxiang Fang, and Zhongyang Luo. 2016. "Preparation and Kinetics of a Heterogeneous Sorbent for CO_2 Capture from the Atmosphere." *Chemical Engineering Journal* 284 (January): 679–86. https://doi.org/10.1016/j.cej.2015.09.009.

Wang, Xia, Linlin Chen, and Qingjie Guo. 2015. "Development of Hybrid Amine-

Functionalized MCM-41 Sorbents for CO_2 capture." *Chemical Engineering Journal* 260: 573–81. https://doi.org/10.1016/j.cej.2014.08.107.

Wheeler, T.A., M.G. Anderson, S.A. Russell, J.E. Woodward, and B.G. Mullinix. 2015. "Application Pressure and Carrier Volume Affects the Concentration of Azoxystrobin on Peanut Foliage and in Soil." *Peanut Science* 42 (2): 128–37. https://doi.org/10.3146/0095-3679-42.2.128.

Yang, J., and C.-H. Lee. 1998. "Adsorption Dynamics of a Layered Bed PSA for H_2 Recovery from Coke Oven Gas." *AIChE Journal* 44 (6): 1325–34. https://doi.org/10.1002/aic.690440610.

Yang, Yun, and Shimin Liu. 2019. "Estimation and Modeling of Pressure-Dependent Gas Diffusion Coefficient for Coal: A Fractal Theory-Based Approach." *Fuel* 253 (October): 588–606. https://doi.org/10.1016/j.fuel.2019.05.009.